



Activation of NLRP3 Inflammasome by Virus-Like Particles of Human Polyomaviruses in Macrophages

Asta Lučiūnaitė^{1*}, Indrė Dalgėdienė¹, Rapolas Žilionis^{1,2}, Kristina Mašalaitė¹, Milda Norkienė¹, Andrius Šinkūnas², Alma Gedvilaitė¹, Indrė Kučinskaitė-Kodžė¹ and Aurelija Žvirblienė¹

¹ Institute of Biotechnology, Life Sciences Center, Vilnius University, Vilnius, Lithuania, ² R&D Department, Droplet Genomics, Vilnius, Lithuania

Viral antigens can activate phagocytes, inducing inflammation, but the mechanisms are barely explored. The aim of this study is to investigate how viral oligomeric proteins of different structures induce inflammatory response in macrophages. Human THP-1 cell line was used to prepare macrophages that were treated with filamentous nucleocapsid-like particles (NLPs) of paramyxoviruses and spherical virus-like particles (VLPs) of human polyomaviruses. The effects of viral proteins on cell viability, pro-inflammatory cytokines' production, and NLRP3 inflammasome activation were investigated. Filamentous NLPs did not induce inflammation while spherical VLPs mediated inflammatory response followed by NLRP3 inflammasome activation. Inhibitors of cathepsins and K⁺ efflux decreased IL-1 β release and cell death, indicating a complex inflammasome activation process. A similar activation pattern was observed in primary human macrophages. Single-cell RNAseq analysis of THP-1 cells revealed several cell activation states different in inflammation-related genes. This study provides new insights into the interaction of viral proteins with immune cells and suggests that structural properties of oligomeric proteins may define cell activation pathways.

Keywords: macrophage, polyomavirus, NLRP3 inflammasome, cathepsins, inflammation

OPEN ACCESS

Edited by:

Giampaola Fantuzzi,
University of Illinois at Chicago,
United States

Reviewed by:

Ka Man Law,
Kaiser Permanente Bernard J Tyson
School of Medicine, United States
Selcan Demir,
Erzurum Regional Research and
Training Hospital, Turkey

*Correspondence:

Asta Lučiūnaitė
asta.luciuinaite@bti.vu.lt

Specialty section:

This article was submitted to
Inflammation,
a section of the journal
Frontiers in Immunology

Received: 08 December 2021

Accepted: 08 February 2022

Published: 09 March 2022

Citation:

Lučiūnaitė A, Dalgėdienė I, Žilionis R, Mašalaitė K, Norkienė M, Šinkūnas A, Gedvilaitė A, Kučinskaitė-Kodžė I and Žvirblienė A (2022) Activation of NLRP3 Inflammasome by Virus-Like Particles of Human Polyomaviruses in Macrophages. *Front. Immunol.* 13:831815. doi: 10.3389/fimmu.2022.831815

INTRODUCTION

The components of innate immunity such as macrophages play a key role in the onset and progression of inflammatory and age-related diseases (1, 2). Macrophages are considered as a potential target for treatment of many diseases; therefore, molecular mechanisms related to their activation are currently a top priority in research (3). Besides, macrophages are known to recognize the structural properties of the activation agents and influence the inflammatory response *via* inflammasome activation (4, 5). Inflammasomes are intracellular protein complexes representing important components of the innate immune system (6). The best-described representative is NLRP3 inflammasome. It contains three major components—nucleotide-binding and oligomerization domain-like receptor, apoptosis-associated speck-like protein containing CARD (ASC), and pro-caspase-1. NLRP3 inflammasome assembly results in IL-1 β release and inflammatory cell death—pyroptosis (7). Endogenous and external factors can trigger its assembly. Activation of NLRP3 inflammasome is associated with various diseases, including gout and Alzheimer's disease (8). Our previous study showed that NLRP3 inflammasome is

activated by amyloid beta (A β), both oligomers and protofibrils (9). Inflammasome activation was also induced by α -synuclein (10) and tau oligomers (11). However, the most explored inflammasome triggers are polymeric nanoparticles (12), cholesterol crystals (13), and airborne pollutants such as silica (14). The structural properties of synthetic nanoparticles determine the outcome of cell activation (15). Previously, we have demonstrated that spherical oligomeric proteins of viral origin induce inflammatory responses in macrophages, but the mechanism and molecular components of this process are not yet confirmed (16). In addition, another study demonstrated that the nucleocapsid (N) protein of Zika virus activated the inflammasome (17). Repetitive and latent viral infections are potential agents of inflammation (18). This frame of reference draws attention to the latent viral infections and their role in inflammation.

It is well known that some viruses lie dormant within the host after an acute infection. According to the World Health Organization, 50%–80% of the world population is infected by polyomaviruses (PyVs) during childhood (19). The effects of these viruses and their antigens on innate immunity throughout life are not fully understood. For example, herpes virus in its latent form can cause multisymptom illnesses with a broad range of simultaneous symptoms, such as cognitive disorders, depression, and fatigue (18). However, the mechanism of multisymptomatic illness is unclear. Investigation of inflammatory responses induced by proteins of viruses causing acute and latent infection may indicate whether these viral proteins alone are capable of activating the immune system.

Inflammasome activation by latent viruses was demonstrated in different viral infections, and it could be related to their deleterious effects. So far, the identified viral triggers of the inflammasome are viral nucleic acids and viroporins, which make pores in cell membranes and disturb ion homeostasis and induce mitochondrial stress or ROS production (20). For example, IFI16 inflammasome is activated by Epstein–Barr virus DNA during its latency (21). IFI16 also senses Kaposi's sarcoma-associated herpesvirus genome (22). This could be a potential mechanism of inflammation associated with Kaposi's sarcoma. In a mouse model, it was demonstrated that mouse cytomegalovirus-induced activation of NLRP3/NLRP1 may contribute to pulmonary fibrosis caused by latent cytomegalovirus infection (23). However, the ability of viral surface antigens and other structural proteins to activate the inflammasome is still insufficiently studied. Another question is whether viral proteins or other factors during their latency are produced, which could mediate inflammation. For example, herpes simplex virus-1 (HSV-1) can induce A β production in infected brain cells in its latent phase (24). Furthermore, these amyloids promote neurotoxicity and neuroinflammation. HSV-1 is known to interact with AD-related genes and proteins (25). There is an increasing number of evidence that A β has a protective function by inhibiting viral replication and virus attachment to neurons (26). In response to HSV-1, neurons start to produce A β to fight infection; however, for genetically susceptible persons, A β accumulation can lead to AD (27, 28). The impact of virus reactivation to neuroinflammation and neurodegeneration in mouse models reveals the role of the

immune system in disease progression (29, 30). Studies show that HSV-1 reactivation promotes cognitive impairment (31, 32). However, processes during viral latency period are less investigated. It was demonstrated that inflammatory cytokines are produced even during viral latency (33, 34).

It is important to investigate how the components of innate and adaptive immunity are activated, including the inflammasome, interferons, and other inflammatory molecules, in viral infections or during vaccination. VLPs are already established as carriers and adjuvants in vaccines. Components of vaccines can activate the inflammasome as it was reported for the ISCOMATRIX adjuvant (35). Studying how different viral proteins especially VLPs stimulate the immune cells would allow the selection of better tools for vaccination.

Inflammatory reactions induced by synthetic polymeric particles in macrophages vary depending on their size and shape (4, 5). Similarly, viral proteins may also determine cellular response depending on their structural properties. Our study was aimed to investigate how recombinant viral proteins induce inflammatory response in macrophages focusing on inflammasome activation. The VLPs derived from major capsid protein VP1 of human PyVs—Karolinska Institute (KI) PyV and Merkel cell (MC) PyV, self-assembling to spherical particles about 20–60 nm in diameter (36)—were selected as typical representatives of spherical oligomeric proteins. The NLPs of measles and mumps viruses were chosen as a model of oligomeric proteins forming filamentous rod-shaped structures (37, 38). We showed that inflammatory responses and activation of NLRP3 inflammasome in macrophages depend on the structural properties of viral proteins. This study provides new insights into the ability of multimeric viral antigens to induce inflammatory response in innate immune cells.

MATERIALS AND METHODS

Materials

Dulbecco's modified Eagle's medium (DMEM; cat# 31966047), Roswell Park Memorial Institute 1640 medium (RPMI, cat#61870044), FluoroBrite DMEM (cat#A1896701), fetal bovine serum (FBS; cat# A3840402), penicillin/streptomycin (P/S; cat#15140122), Dulbecco's Phosphate Buffered Saline (PBS; cat#14190250), and cell dissociation reagent TrypLE™ Express Enzyme (cat#12604021) were obtained from Gibco, Thermo Fisher Scientific. Cell culture plates: T75 culture flasks Cell Culture Treated EasYFlasks (cat#156499) were from Nunc, Thermo Fisher Scientific; TPP Multi-well tissue culture plates (cat# 92012, cat#92024, cat#92048) were from TPP Techno Plastic Products AG; IbiTreat 96-well μ -plates (cat#89626) were from Ibi. LPS (cat#tlrl-ebllps), nigericin (cat#tlrnig), MCC950 (cat#inh-mcc), normocin (cat#ant-nr-1), and zeocin (cat#ant-zn-05) were from InvivoGen. K777 [K11777] (cat#AG-CR1-0158-M001) was from Adipogen. CA-074 Me (cat#A8239) was from ApexBio Technology. LDH cytotoxicity detection kit (cat#11644793001) was from Roche Diagnostics, Sigma-Aldrich

by Merck. Phorbol 12-myristate 13-acetate (PMA, cat# P1585-1MG) was obtained from Sigma-Aldrich by Merck. Propidium iodide (PI; cat#638), Hoechst33342 (Hoechst, cat#639), and FAM-FLICA[®] Caspase-1 Assay Kit (containing FLICA reagent FAM-YVAD-FMK—caspase-1 inhibitor probe; cat#98) were obtained from ImmunoChemistry Technologies. Dimethylsulfoxide (DMSO; cat#A3672) was from PanReac AppliChem and the ITW Reagents. Human IL-1 beta Uncoated ELISA Kit (cat# 88-7261-77) and TNF alpha Uncoated ELISA Kit (cat#88-7346-86), IL-6 Uncoated ELISA Kit (cat#88-7066), IL-10 Uncoated ELISA Kit (cat#88-7106), Phosphate-Buffered Saline (10×), pH 7.4 (cat#AM9624), and UltraPure DNase/RNase-Free Distilled Water (cat#10977035) were from Invitrogen, Thermo Fisher Scientific. Tween-20 (cat# 9127.1) and sulfuric acid (H₂SO₄, cat#X873.1) were from Carl Roth. Chemiluminescent substrate—SuperSignal West Femto Maximum Sensitivity Substrate (cat#34094) was from Thermo Fisher Scientific. NextSeq 500/550 High Output Kit v2.5 (cat#20024906) was obtained from Illumina. Recombinant mumps (cat#12MuNP-ASc-Gly-C) and measles (cat#12MeN-BSc-Gly-C) N proteins were from Baltymas (Lithuania).

Cell Lines

Human cell line THP-1 was kindly provided by Prof. Linas Mažutis (Vilnius University, Vilnius, Lithuania). Cells were propagated in RPMI 1640 + 10% FBS + 100 U/ml of P/S and were split twice a week by a ratio of 1:5 to 1:10.

Human cell line THP-1 monocytes—ASC speck reporter cells were purchased from Invivogen (#thp-ascgfp, Invivogen, France) and called THP-1-ASC-GFP. These cells express ASC protein fused to GFP. Cells were propagated in RPMI 1640 + 10% FBS + 100 U/ml of P/S + 100 µg/ml of zeocin + 100 µg/ml normocin and were split twice a week by a ratio of 1:5 to 1:10. During cell differentiation to macrophages and treatment, zeocin and normocin were not used.

Human Macrophage Cell Culture

Human macrophage cell cultures were prepared by differentiation of THP-1 cells (39). The cells were seeded in the 24-well plate at a density of 0.125×10^6 /well using RPMI 1640 medium supplemented with 10% FBS and 1% P/S and differentiated to macrophages using 100 ng/ml of PMA. After 48 h of differentiation, the medium was replaced with the fresh medium without PMA and cells were left to rest for another 24 h. After the rest period, the cells are differentiated into macrophages and were used in experiments with viral proteins. These macrophage-like cells were used in the study and called THP-1 macrophages.

THP-1 macrophages were washed once with serum-free RPMI and treated with viral proteins for 24 h. Viral proteins were prepared in PBS, so control when PBS was added instead of viral proteins was used. As a positive control, the inflammasome inducer nigericin was used at 10 µM concentration. MCC950, which selectively inhibits the NLRP3 inflammasome, was used at 1 µM concentration and added 30 min before the treatment. Inhibitors of cathepsins were used with the following concentrations: CA-074 Me at 2 µM and 10 µM, and K777 at 15 µM, added 30 min before the treatment. Another inhibitor,

glibenclamide, which blocks K⁺ efflux, was used at 50 µM concentration, 30 min before the treatment. After incubation, cell culture supernatants were collected and stored at −20°C for further cytokine analysis. Supernatants for LDH assay were used instantly.

Primary human macrophages were purchased from Lonza (#4W-700). Human macrophages were derived from CD14⁺ human monocytes of one donor. Cryopreserved cells were thawed and cultured for 2 days in RPMI 1640 medium supplemented with 10% FBS and 1% P/S before treatment. The cells were treated as THP-1 macrophages in serum-free RPMI. Cells for FLICA assay were plated in an Ibidi 96-well µ-plate and for ELISA in a TPP 24-well plate.

Viral Proteins

Macrophages were activated with recombinant viral proteins (20 µg/ml) representing various oligomeric shapes and forms. KI polyomavirus recombinant major capsid protein VP1 (KIPyV VP1, 41.6 kDa) forms spherical oligomers—VLPs—containing up to 360 monomers as described previously (36). MC polyomavirus recombinant major capsid protein VP1 (MCPyV VP1, 46.6 kDa) forms spherical oligomers—VLPs, containing up to 360 monomers as described previously (36). Measles virus recombinant nucleocapsid protein (MeV N, 58.0 kDa) forms filamentous structures as described previously (37, 38). Mumps virus recombinant nucleocapsid protein (MuV N, 66 kDa) also forms filamentous structures as described previously (40). All viral proteins were expressed in yeast expression system and purified by CsCl density gradient centrifugation (36, 37, 40, 41).

VLP Production, Purification, and Analysis

Purification of VLPs of recombinant PyV VP1 proteins and electron microscopy were carried out as described previously (36). Briefly, *Saccharomyces cerevisiae* yeast biomass after the induction of recombinant proteins synthesis was mechanically homogenized in DB450 buffer (450 mM NaCl, 1 mM CaCl₂, 0.25 M L-Arginine, and 0.001% Triton X-100 in 10 mM Tris/HCl buffer, pH 7.2) with 2 mM PMSF and EDTA-free Complete Protease Inhibitors Cocktail tablets (Roche Diagnostics, Mannheim, Germany), and its supernatant was transferred onto 30%–60% sucrose gradient. After overnight centrifugation (at 4°C) at 100,000×g (Beckman Coulter Optima L-90 ultracentrifuge), collected 2-ml fractions were analyzed by SDS-PAGE. The mixture of fractions containing PyV VP1 proteins diluted in DB150 buffer (150 mM NaCl, 1 mM CaCl₂, 0.25 M L-Arginine, and 0.001% Triton X-100 in 10 mM Tris/HCl buffer, pH 7.2) and VLPs were concentrated by ultracentrifugation at 100,000×g for 4 h (at 4°C). Thereafter, pellets containing VP1 were subjected to ultracentrifugation overnight on CsCl gradient (1.23–1.46 g/ml density) at 4°C. One-milliliter fractions of formed gradient were collected and analyzed by SDS-PAGE. Positive fractions were pooled, diluted in DB150 buffer, and concentrated as described above. The isolated VLPs were dissolved in PBS, dialyzed, and stored in PBS with 50% glycerol. The VLP formation was verified by examination of the purified proteins using Morgagni-268 electron microscope (FEI, Inc., Hillsboro, OR, USA). The protein samples were placed on 400-mesh carbon-coated

palladium grids (Agar Scientific, Stansted, UK) and stained with 2% aqueous uranyl acetate.

Cell Cytotoxicity Assays

Cell cytotoxicity was measured using lactate dehydrogenase (LDH) release assay (LDH cytotoxicity detection Kit). A quantity of 50 μ l of cell supernatants was used to perform the cytotoxicity assay according to the manufacturer's protocol. Briefly, 50 μ l of supernatant was mixed with freshly prepared LDH reagent and incubated at 37°C. After 30 min, absorbance was measured at 490 nm using a Multiskan GO microplate spectrophotometer (Thermo Fisher Scientific Oy, Finland).

To determine cell viability, PI/Hoechst nuclear staining was also used. Nuclei were stained with 1.25 μ g/ml PI and 1 μ g/ml Hoechst33342 in cell culture medium for 30 min. The cells were washed with PBS. The fluorescence signal was measured by taking photos automatically with an EVOS FL Auto fluorescence microscope. Images were taken using a 20 \times objective. Viability was quantified according to a ratio of PI (dead cells) and Hoechst (all cells), expressed in percentages.

Quantitation of Cytokines in Cell Culture Supernatants

ELISA kits for the measurement of human cytokine—IL-6, IL-10, IL-1 β , and TNF- α —levels in cell culture supernatants were used (#88-7066, #88-7106, #88-7261, and #88-7346, Thermo Fisher Scientific, USA). ELISA kits are based on the sandwich immunoassay technique. Supernatants were used diluted up to 1:600. All procedures were performed according to the manufacturer's protocols. In the last step, 3,3',5,5'-tetramethylbenzidine (TMB) substrate solution was added to each well. The plates were monitored for 15 min for color development, the reaction in wells was stopped with 3.6% H₂SO₄ solution, and the wells were read at 450 nm with reference wavelength at 620 nm using a Multiskan GO microplate spectrophotometer. A standard curve was generated from cytokine standard, and the cytokine concentration in the samples was calculated.

Detection of ASC Speck Formation in THP-1 Macrophages

THP-1 monocytes expressing ASC fused with green fluorescent protein (GFP) was used for ASC speck formation. The cells were cultivated in RPMI 1640 medium supplemented with 10% FBS, 1% P/S, 100 μ g/ml normocin, and 100 μ g/ml selective antibiotic zeocin. THP-1-ASC-GFP cells were differentiated to macrophages as origin THP-1 using RPMI 1640 medium supplemented with 10% FBS, 1% P/S, and PMA. THP-1-ASC-GFP macrophages were treated with viral proteins in serum-free RPMI. Thirty minutes before the treatment termination, Hoechst33342 was added to stain cell nuclei. After 24 h of treatment, cell culture medium was replaced with FluoroBrite DMEM. ASC specks were analyzed with an EVOS FL Auto fluorescence microscope (Life Technologies, USA) by taking photos with 20 \times objective. Cells were counted according to the number of nuclei. ASC speck number per cell was counted using the image processing program ImageJ.

Measurement of Active Caspase-1

Active caspase-1 was detected using Fluorochrome Labeled Inhibitors of Caspases (FLICA) assay according to the manufacturer's protocol. Briefly, FLICA reagent (FAM-YVAD-FMK—caspase-1 inhibitor probe) was added after the 15-h treatment with viral proteins and incubated for 1 h. Cells were washed three times and stained with Hoechst33342 at 1 μ g/ml and PI at 1.25 μ g/ml. After washing, cells were analyzed directly by an EVOS FL Auto fluorescence microscope using a 20 \times or 40 \times objective.

SDS-PAGE and Western Blot Analysis

To determine cleaved caspase-1 p20 fragment, Western blot assay (WB) was performed. After cell treatment with viral proteins, supernatant was collected and centrifuged at 600 \times g for 10 min to remove cellular debris. Then, the protein content of the supernatants was concentrated 10 \times using centrifugal filters with a 10-kDa cutoff (#UFC501096, Amicon, Merck). The concentrated samples were boiled in a reducing sample buffer and separated in 4%–12% polyacrylamide gel (#NW04122BOX, Thermo Fisher Scientific) electrophoresis (PAGE) in MES SDS running buffer (#B0002 Invitrogen, Thermo Fisher Scientific). The proteins from the SDS-PAGE gel were blotted onto a 0.2- μ m nitrocellulose (NC) membrane (#LC2000, Invitrogen, Thermo Fisher Scientific) by wet transfer. The membrane was blocked with 5% BSA in PBS for 1 h at RT and rinsed with TBST. The membrane was then incubated with primary antibodies in TBST with 1% BSA overnight at 4°C. The primary antibodies against human caspase-1 (clone Bally-1, #AG-20B-0048-C100, RRID: AB_2490257, Adipogene) were used at 1:1,000 dilution. Thereafter, the membrane was incubated with secondary antibodies Goat Anti-Mouse IgG (H+L)-HRP Conjugate (Bio-Rad) diluted 1:5,000 in TBST with 1% BSA for 1 h at RT. The horseradish peroxidase (HRP) enzymatic reaction was developed using chemiluminescent substrate (#34094, Thermo Fisher Scientific).

Immunocytochemistry for Studying the Uptake of VLPs by Macrophages

Cells were stained in IbiDITreat 96-well μ -plates. After the treatment, cells were washed with PBS and fixed in 4% PFA dissolved in PBS for 15 min and permeabilized with 0.1% Triton X-100 prepared in PBS for 10 min. Blocking solution—PBS containing 2% BSA—was applied for 30 min followed by two washing steps. The primary antibodies rabbit polyclonal anti-CD68 (1:100; #25747-1-AP, RRID : AB_2721140, Proteintech) and mouse anti-PyV VP1 VLPs (monoclonal antibodies of hybridoma supernatant at dilution 1:2) were added to the blocking solution and incubated overnight. The following secondary antibodies were respectively used: goat anti-rabbit (1:1,000) and goat anti-mouse (1:1,000). The secondary antibodies were applied for 2 h followed by two washing steps. Hoechst33342 was used for nuclear staining at 1 μ g/ml for 30 min in PBS. The images were taken using a 40 \times objective. CD68 was used as a macrophage and lysosomal marker. The experiment was imaged using an EVOS FL Auto fluorescence microscope (Thermo Fisher Scientific, USA). Acquired images

were processed using ImageJ (Wayne Rusband; National Institute of Health, Bethesda, MD, USA).

For the immunocytochemistry, in-house generated murine MAbs against recombinant NLPs and VLPs were used (#MAB clone—virus antigen indicated): #7C11—MeV N (38); #5E3—MuV N (40); #5G8—KIPyV VP1; and #11A2—MCPyV VP1.

Microscopy

All images were taken with fluorescence microscope EVOS FL Auto (#AMAFD1000, Thermo Fisher Scientific). EVOS imaging systems use LED light cubes, which combine bright LED illumination with excitation and emission filters into single components. PI signal was detected in RFP light cube; Hoechst33342 signal—in DAPI light cube (AMEP#4650); GFP and AlexaFluor 488 signal—in GFP light cube (AMEP#4651); PI signal—in RFP light cube (AMEP#4652); AlexaFluor 594 signal—in TxRed light cube (AMEP#4655). The following objective lenses were used 20× (#AMEP4682) and 40× (#AMEP4683). Acquisition software EVOS[®] FL Auto v1.6 was used. Images were prepared with ImageJ program. Firstly, appropriate pseudo-color was added at images of 8-bit format. Then, the images were converted to RGB color format. Finally, brightness and contrast were adjusted equally to all images per channel. Images (fluorescent signal and object counting) were analyzed with ImageJ. The final figures were arranged using Adobe Photoshop without any brightness/contrast and color manipulations.

Cell Preparation for Single-Cell RNA Sequencing

THP-1 macrophages for RNA sequencing analysis were treated for 15 h with PyV-derived VLPs (20 µg/ml). After the treatment, cells were washed with PBS and detached with TrypLE reagent after 15 min of incubation at a cell culture incubator (37°C, 5% CO₂). After centrifugation, cells were washed twice with 1× RNase-free PBS (cat#AM9624, Invitrogen). After final centrifugation, cells were resuspended in RNase-free PBS and kept on ice till cell preparation for RNA sequencing analysis

Single-Cell RNA Sequencing

Single-cell RNA sequencing (scRNAseq) was performed using a modified version of the inDrops method (42, 43). While the original version is based on the CEL-Seq protocol (44) that involves linear cDNA amplification by *in vitro* transcription, the modified version relies on template switching and cDNA amplification by PCR, as in the Smart-seq protocol (45). First, single-cell transcriptomes were barcoded in 1-nl droplets by co-encapsulating: (i) barcoding hydrogel beads; (ii) the reverse-transcription/lysis (RT/lysis) mix; and (iii) the cell suspension. Cell encapsulation was performed using the microfluidic device described in (43) on an Onyx platform (Droplet Genomics). Maxima H- minus (Thermo Fisher, cat. no. EP0751) was used for reverse transcription with template switching. RT was performed for 1 h at 42°C followed by heat inactivation for 5 min at 85°C. The emulsion was then broken and the pooled material was taken through library preparation for Illumina sequencing, which involves the following steps: (i) cDNA amplification (Terra PCR direct Polymerase, Takara, cat. no. 639270),

(ii) fragmentation and adapter ligation (NEBNext[®] Ultra[™] II FS DNA Library Prep Kit for Illumina, NEB, cat. no. E7805S), and (iii) indexing PCR (KAPA HiFi HotStart ReadyMix PCR Kit, Roche, cat. no. KK2601). Sequencing was performed on a single Illumina NextSeq run (NextSeq 500/550 High Output Kit v2.5 (75 Cycles), Illumina, cat. no. 20024906).

ScRNAseq Raw Data Processing

The solo-in-drops pipeline (<https://github.com/jsimonas/solo-in-drops>), which is a wrapper around STARsolo (<https://github.com/alexdobin/STAR/blob/master/docs/STARsolo.md>), was used to obtain cells × genes expression matrices. STARsolo expects as input two fastq files per library, one containing the barcode information and the other the transcript information. Meanwhile, the custom scRNAseq protocol used in the current study outputs 3 fastq files per library: barcode half 1, barcode half 2, and transcript. Solo-in-drops prepares the data for compatibility with STARsolo. STAR (version 2.7.6a) was run with the following parameters: – soloType CB_UMI_Simple, – soloUMIfiltering MultiGeneUMI, and – soloCBmatchWltype IMM_multi_pseudocounts. *Homo sapiens* (human) genome assembly GRCh38 (hg38) was used as the reference.

ScRNAseq Count Data Analysis

Jupyter notebooks with commented code for scRNAseq data analyses, including data filtering, normalization, visualization, clustering, cell population annotation, differential gene expression (DGE) analysis, cell cycle scoring, and plots used in **Figures 8–10** and **Supplementary Figures 4–6** are provided on GitHub (github.com/rapolaszilionis/Luciunaite_et_al_2022). The Scanpy toolbox was used for data analysis. Transcriptomes with fewer than 900 total counts were excluded. No filtering on the fraction of mitochondrial counts was performed. UMAP (46) was used for data visualization in 2D. Leiden clustering was used to divide the graph into clusters, which were annotated based on their gene expression profiles. Gene Ontology (GO) gene set enrichment analysis (**Figures 8D** and **10E**) was performed using the tool available online (<http://geneontology.org>) using Panther GO-Slim Biological Processes as the annotation data set. For DGE analyses (**Figure 9C**, **10E**), the Mann–Whitney *U* test was used to test for significance, and the Benjamini–Hochberg procedure was used to correct for multiple hypothesis testing.

Statistical Analysis

All statistical analyses were performed with GraphPad Prism 9.2.0 (GraphPad Software, Inc., La Jolla, CA). The data in the figures are represented as individual data points from at least 6 independent experiments using box plots (showing minimum, first quartile, median, third quartile, and maximum) or bar graphs. Independent experiments referred to as *N* means the number of independent cell culture preparations and *n* means the number of technical repeats. Normality test was carried out to test if the values come from a Gaussian distribution. Statistical comparisons of vehicle controls versus treatment were performed with one-way ANOVA in conjunction with a Tukey's multiple comparison test or Student's *t*-test. A Kruskal–Wallis test with Dunn's *post hoc* test was used for

non-parametric data. Differences with p value less than 0.05 were considered to be statistically significant: * $p < 0.05$, ** $p < 0.01$, *** $p < 0.001$, **** $p < 0.0001$. To emphasize non-significant results, ns was used.

RESULTS

We investigated the ability of viral multimeric proteins to induce inflammatory response in macrophages focusing on inflammasome activation. For this study, we have selected structurally diverse viral proteins: filamentous NLPs of measles and mumps viruses (*Paramyxoviridae* family) that usually cause acute infections, and spherical VLPs derived from VP1 of PyVs (*Polyomaviridae* family) that generally induce latent viral infections. We also investigated whether viral oligomeric proteins of diverse structure can determine different patterns of cell activation.

NLPs Did Not Activate THP-1 Macrophages Despite Their Interaction With the Cells

First at all, we investigated the uptake of viral proteins by THP-1 macrophages. The cells were treated with recombinant NLPs of measles and mumps viruses, as well as recombinant PyV VLP, for 24 h to observe the uptake of multimeric viral proteins. The NLPs and VLPs were immunostained with the respective monoclonal antibodies. We also immunostained the cells for the macrophage and lysosomal marker CD68. The uptake of both NLPs and VLPs was detected microscopically demonstrating their interaction with THP-1 macrophages (Figure 1A).

To investigate macrophage activation by multimeric viral proteins, we started with recombinant NLPs of measles and mumps viruses forming filamentous structures. These NLPs are long rod-shaped structures, about 20 nm in diameter, mimicking the nucleocapsids of native viruses (40, 41). The NLPs were not cytotoxic to THP-1 macrophages according to propidium iodide (PI) and Hoechst nuclear staining assay (Figures 1B, C) and lactate dehydrogenase (LDH) release (Figure 1D). Treatment of THP-1 macrophages with NLPs did not cause any inflammatory response according to TNF- α release data (Figure 1E). The NLPs also did not activate the inflammasome as no change in IL-1 β secretion (Figure 1F) was detected. We concluded that NLPs have no effect on inflammatory response.

PyV-Derived VLPs Induced Inflammatory Response Followed by NLRP3 Inflammasome Activation in THP-1 Macrophages

Next, we investigated macrophage activation by PyV-derived VLPs of spherical structures that are similar to native viruses in their shape and size. In order to evaluate the effects of diverse VLPs, we have selected PyV-derived VLPs of different sizes, ranging 20–60 nm in diameter (36). KIPyV proteins VP1 form heterogeneous VLPs, ranging from 20 to 60 nm, while MCPyV proteins VP1 form more homogeneous VLPs, 45–50 nm in

diameter. Thus, we investigated VLPs of different sizes. Treatment of human THP-1 macrophages with PyV-derived VLPs induced cell activation and inflammatory response according to TNF- α and IL-6 release (Figures 2A, B). Therefore, we assumed that VLPs activated the NF- κ B signaling pathway, which could be a priming step for further inflammasome activation. In addition, we assayed the cells for anti-inflammatory cytokine IL-10 secretion and did not detect its release after VLP treatment (detected IL-10 values were below the assay detection limit). PyV-derived VLPs induced not only secretion of inflammatory cytokines but also provoked cell death as LDH release was increased (Figure 2D) and dead cells were detected using PI staining (Figure 2E). We also demonstrated that VLPs of different sizes induced cell activation signal of different strength. Large-sized (45–50 nm in diameter) homogeneous MCPyV VLPs induced higher inflammatory response as compared to heterogeneous KIPyV VLPs (Figure 2).

Then, we assessed whether PyV-derived VLPs induce activation of NLRP3 inflammasome in THP-1 macrophages. To test this, we used a small-molecule MCC950, which specifically inhibits NLRP3 inflammasome. PyV-derived VLPs induced cell death (Figures 2D, E) and IL-1 β release, showing inflammasome activation (Figure 2C). Pre-treatment with MCC950 inhibitor before adding the VLPs significantly decreased this activation signal (Figures 2C–E). The inhibitor MCC950 did not influence the secretion level of other inflammatory cytokine TNF- α showing the specificity of inhibitor to inflammasome activation (Figure 2A). These data demonstrate that VLPs are potent inflammatory agents triggering inflammatory cytokine secretion and pyroptotic cell death to a similar extent as classical NLRP3 inflammasome activator nigericin (Supplementary Figure 1).

In the next step, we investigated the formation of ASC specks that would indicate the assembly of the inflammasome. To detect ASC specks, we used THP-1-ASC-GFP macrophages. We identified ASC specks after treating cells with PyV-derived VLPs (Figures 3A, B). However, MCC950 did not fully inhibit ASC speck formation (Figure 3B), which might be explained by ASC speck release from the inflammasome-activated cells. Secreted ASC specks can promote further maturation of inflammatory cytokines (47). In addition, ASC specks could induce a subsequent inflammatory response by activating the surrounding cells.

Next, we performed time-lapse experiments to observe the dynamics of cell activation by PyV-derived VLPs. We took the microscopy images of THP-1-ASC-GFP within 3–24 h fluorescence of treatment with VLPs. The cell activation started to be seen at 12 h, and after 24 h, ASC specks were evidently observed (Supplementary Figure 2A). We also took the images after 14–24 h treatment with VLPs (Figure 3D). There were no differences in green intensity and ASC speck formation within this time interval. We measured LDH release in wild-type THP-1 cells treated with VLPs for 15–23 h. Again, we did not find considerable differences within the 15–23 h treatment period (Figure 3C). We concluded that THP-1 macrophages are activated at about 15 h after VLP addition and their activation pattern remains constant from this time point.

There was a different pattern of cell activation by VLPs and nigericin used as a positive control. In the first hours of nigericin

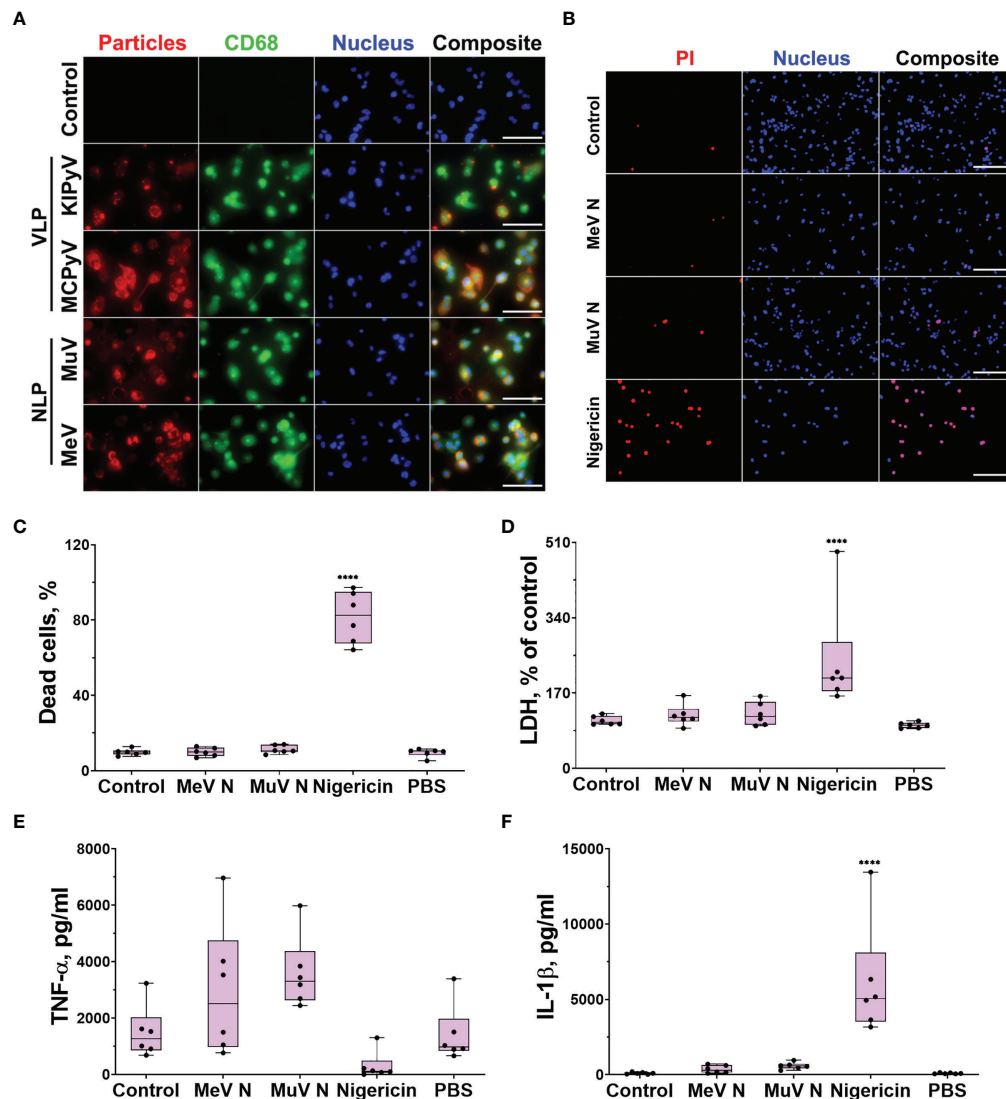


FIGURE 1 | PyV-derived VLPs and NLPs of measles and mumps viruses were taken up by THP-1 macrophages; however, NLPs did not induce cell activation. THP-1 macrophages were treated with recombinant viral proteins (20 $\mu\text{g}/\text{ml}$) for 24 h. Nigericin (10 μM) was used as a positive control. **(A)** Cells were immunostained with anti-NLP and anti-VLP monoclonal antibodies (red), anti-CD68-macrophage and lysosomal marker (green), nuclear stain Hoechst33342 (blue) and analyzed by fluorescence microscopy. The negative control—secondary antibody alone is referred as a control. Images were taken using 40 \times objective. The scale bars indicate 100 μm . Representative images of one experiment are shown. **(B)** PI (dead cells) and Hoechst (all cells) nuclear staining. Images were taken using 20 \times objective. The scale bars indicate 200 μm . **(C)** Quantification of dead cells. **(D)** Cytotoxicity assessed by LDH assay. **(E)** TNF- α and **(F)** IL-1 β secretion determined by ELISA. Data are represented using box plots, **** $p < 0.0001$, one-way ANOVA followed by Tukey's multiple comparison test; stars show statistically significant results compared to control.

treatment, we have observed caspase-1 expression and ASC speck formation (**Supplementary Figures 2B, 3C**). However, the number of ASC speck-positive cells decreased in time and no ASC specks were detected 24 h after nigericin treatment. In contrast, VLPs induced the formation of ASC specks after 15 h (**Figure 3D**), and the signal did not change within the 15–24 h period of VLP treatment.

To prove VLP-induced activation of the inflammasome, we assayed for active caspase-1, which is a major component of the inflammasome cascade, converting pro-IL-1 β to its mature form.

Having the time-lapse experiment data, we collected cell culture supernatant for caspase-1 assay after 15 h—from the steady cell activation time point in order not to lose the active enzyme. The cleaved caspase-1 p20 fragment was detected by WB after THP-1 treatment with VLPs (**Figures 4A, B** and **Supplementary Figure 3**). NLRP3 inhibitor MCC950 reduced generation of the activated caspase-1. Then, we analyzed caspase-1 activation at a single-cell level using FLICA reagent. It contains FAM-YVAD-FMK caspase-1 inhibitor probe, which covalently binds to only activated caspase-1. We revealed caspase-1 activation in

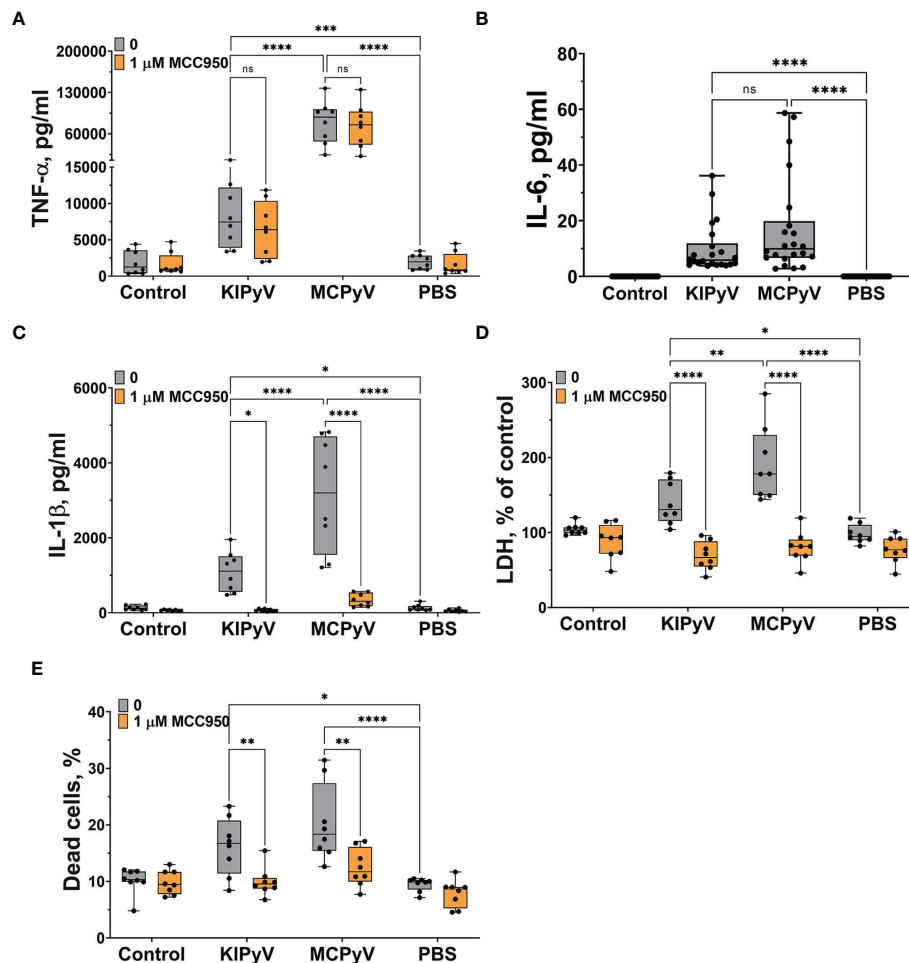


FIGURE 2 | PyV-derived VLPs induced release of inflammatory cytokines TNF- α and IL-6 and activated NLRP3 inflammasome in human THP-1 macrophages. Macrophages were treated with PyV-derived VLPs (20 μ g/ml) for 24 h. Inhibitor MCC950 (1 μ M) was added 30 min before treatment. **(A)** TNF- α , **(B)** IL-6, and **(C)** IL-1 β secretion determined by ELISA. Cytotoxicity assessed by **(D)** LDH assay and **(E)** PI and Hoechst nuclear staining. PI indicates dead cells (red) and Hoechst stains all cell nuclei (blue). Data are represented using box plots with dots showing independent experiments, * $p < 0.05$, ** $p < 0.01$, *** $p < 0.001$, **** $p < 0.0001$, one-way ANOVA followed by Tukey's multiple comparison test; ns, not statistically significant.

some THP-1 macrophages after treatment with VLPs (**Figures 4C, D**). Inflammasome inhibitor MCC950 reduced the level of activated caspase-1. We also stained VLP-treated cells with PI to identify dead cells. Activated caspase-1 co-localized with dead cells confirming the pyroptotic cell death and inflammasome activation.

The Mechanism of VLP-Mediated Inflammasome Activation Is Related to Lysosomal Damage

We further investigated the mechanism of inflammasome activation by PyV-derived VLPs. It is likely that accumulation of phagocytosed VLPs in lysosomes can damage them and induce the release of cathepsins, in particular cathepsin B (CtsB), which is one of the activators of NLRP3 inflammasome. We observed a significant decrease of IL-1 β secretion after treatment of THP-1 cells with CtsB inhibitor Ca-074 Me (**Figure 5A**). However, CtsB

did not reduce cell death (**Figures 5B, C**). The results were the same even at higher (10 μ M) Ca-074 Me concentration (**Figures 5D, E**). This suggests that VLPs may induce the cytotoxicity by a different mechanism next to lysosomal damage-associated cell death.

Then, we treated THP-1 cells with the pan-cathepsins inhibitor K777. We observed a significant decrease in cell death (**Figure 5F**) according to LDH assay. Staining of cell nuclei with PI confirmed that the K777 inhibitor prevented cell death (**Figure 5G**). Next, we measured IL-1 β release and found that K777 significantly suppressed IL-1 β secretion (**Figure 5H**), but not to control baseline. This indicates that K777 is a partial inhibitor of inflammasome activation induced by VLPs.

PyV-Derived VLPs Induced Inflammasome Activation *via* K⁺ Efflux

Lysosomal damage can induce further processes, which consolidate inflammasome activation by VLPs as it was shown

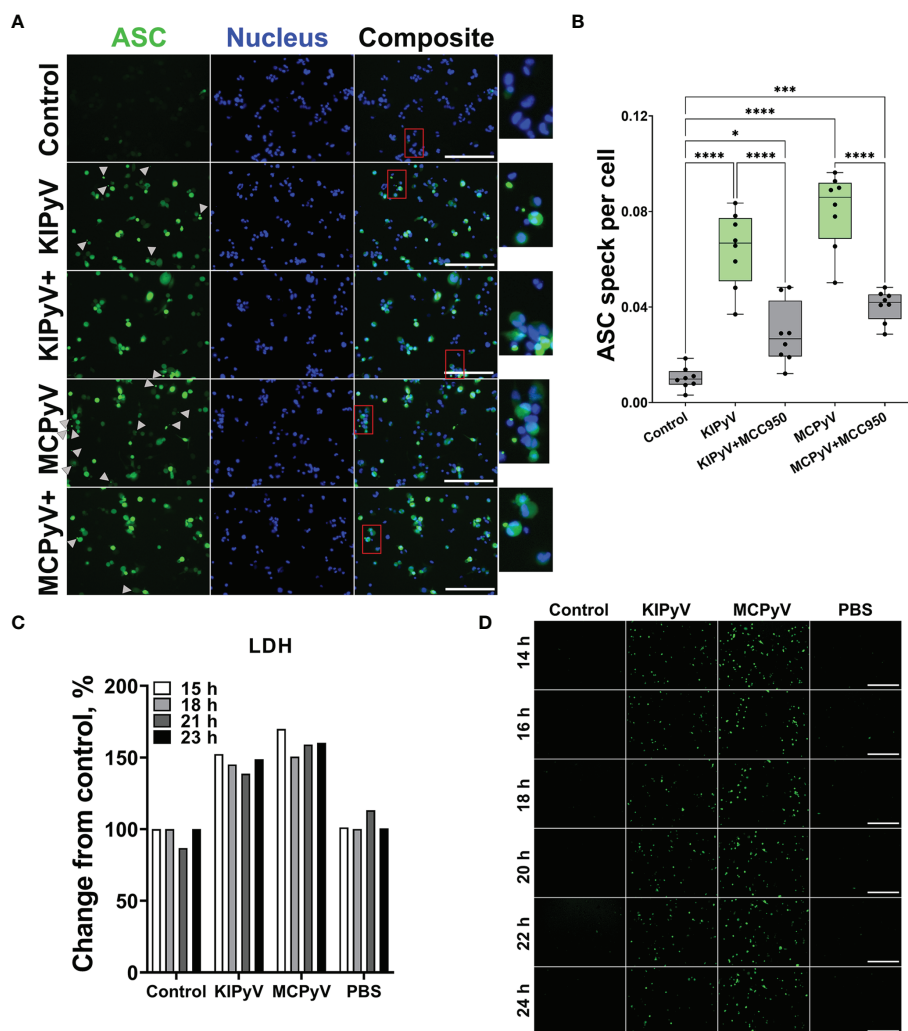


FIGURE 3 | PyV-derived VLPs induced ASC speck formation in human THP-1 macrophages. THP-1-ASC-GFP macrophages were treated for 24 h with PyV-derived VLPs (20 µg/ml); inhibitor MCC950 (1 µM) was added 30 min before treatment. **(A)** Formation of ASC specks was visualized by a fluorescence microscope. Representative images of one experiment are shown. Gray arrows show ASC specks. Red rectangles show magnified parts. “+” refers to MCC950 pre-treatment. The images were taken using 20× objective. The scale bars indicate 200 µm. **(B)** Quantification of ASC speck count per cell. Data are represented using box plots with dots showing independent experiments, * $p < 0.05$, *** $p < 0.001$, **** $p < 0.0001$, one-way ANOVA followed by Tukey’s multiple comparison test. **(C, D)** Time lapse of PyV VLP-induced cell activation. **(C)** LDH assay performed on cell culture supernatant in wild-type THP-1 macrophages. **(D)** The formation of ASC specks detected in THP-1-ASC-GFP. Representative images of one experiment are shown. $N = 1$.

with inhaled particles, like silica and polystyrene nanoparticles (5). The VLPs might also trigger different cell activation pathways leading to inflammasome activation. To prove this assumption, we investigated an alternative inflammasome activation pathway using the K^+ efflux inhibitor, glibenclamide. It significantly blocked cell death (Figure 6A). We also observed a significant decrease in IL-1 β release after glibenclamide pre-treatment (Figure 6B).

Taken together, these results reveal the complexity of inflammatory responses leading to inflammasome activation induced by PyV-derived VLPs in THP-1 macrophages. It is likely that several different mechanisms are involved in this process.

Inflammasome Activation by PyV-Derived VLPs Was Confirmed in Primary Human Macrophages

As cell lines may misrepresent real cell activation pattern, we used primary human macrophages derived from monocytes of peripheral blood mononuclear cells to confirm cell activation profile observed in THP-1 cells treated with PyV-derived VLPs. Activation of primary human macrophages with VLPs revealed a similar cell activation pattern to that observed in THP-1 macrophages—a significant increase in activated caspase-1 (Figures 7A, B), cell death (Figure 7C), and TNF- α and IL-1 β release (Figures 7D, E). Moreover, NLRP3 inflammasome inhibitor MCC950 significantly reduced primary human macrophage

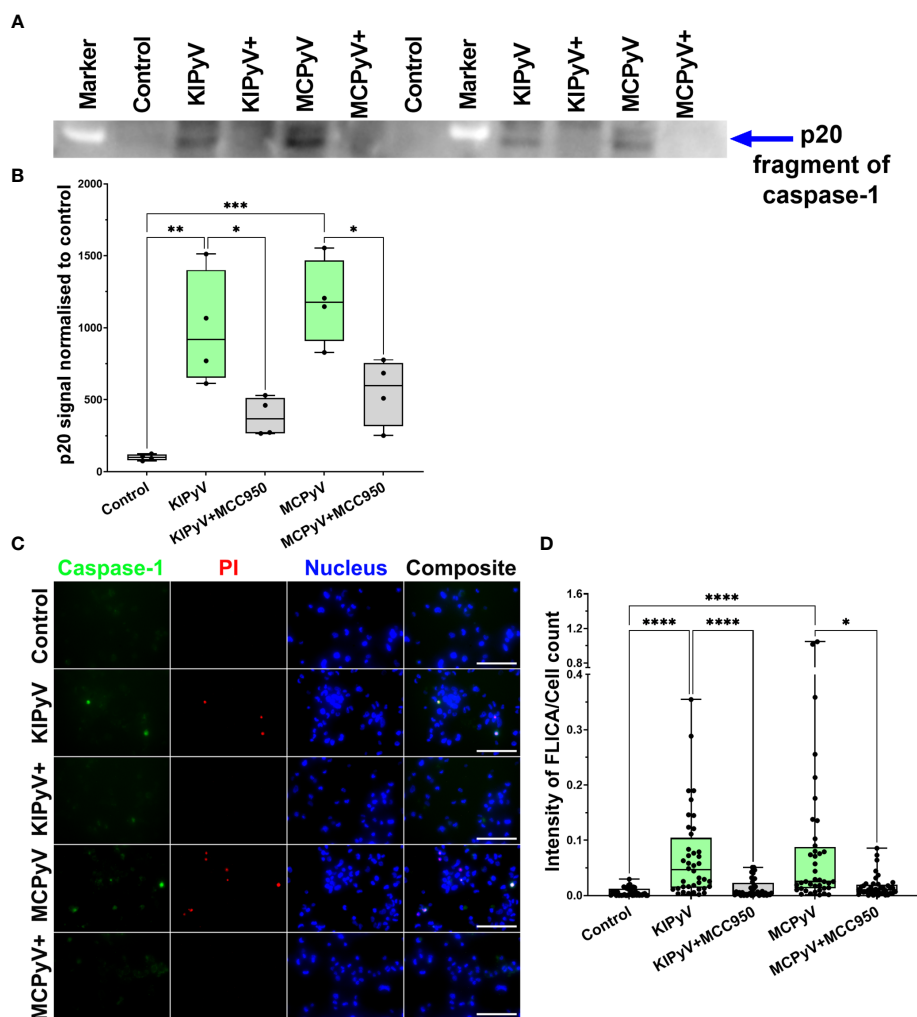


FIGURE 4 | PyV-derived VLPs induced caspase-1 activation in human THP-1 macrophages. Macrophages were treated for 15 h with PyV-derived VLPs (20 $\mu\text{g/ml}$); inhibitor MCC950 (1 μM) was added 30 min before treatment. **(A)** Cleaved caspase-1 was determined in cell supernatants by WB. The WB fragment of cleaved caspase-1 (p20 fragment) is shown. See **Supplementary Figure 3** for full WB image. "+" refers to MCC950 pre-treatment. Duplicates of one experiment are shown. **(B)** Quantification of p20 fragment of caspase-1; duplicates of each experiments were quantified, $N=2$. **(C)** Representative images of the activated caspase-1 staining by FLICA (green) reagent. Dead cell nuclear stain PI (red) and nuclear stain Hoechst (blue) was used. The images were taken using 20 \times objective. The scale bars indicate 100 μm . **(D)** Caspase-1 quantification according to FLICA analysis, $n=40$ photos per condition. $N=1$. Data are represented using box plots showing number of photos and analyzed by Kruskal–Wallis test with Dunn's *post hoc*, * $p < 0.05$, ** $p < 0.01$, *** $p < 0.001$, **** $p < 0.0001$.

activation and rescued from cell death (**Figures 7A–C**). As in experiments with THP-1 macrophages, not all primary human macrophages were activated by the VLPs, and the percentage of dead cells did not exceed 20% (**Figures 2E** and **7C**). According to FLICA assay indicating caspase-1 activation (**Figures 7A, B**), only a part of primary human macrophages was activated by VLPs. According to PI staining, primary macrophages having activated caspase-1 also were dead (**Figure 7A**) proving the pyroptotic cell death. These experiments indicate a similar pattern of PyV VLP-induced inflammation followed by inflammasome activation both in THP-1 cell line and in primary human macrophages.

We found that in some THP-1 cells, the inflammasome is activated, and in some, it is not based on data obtained from

caspase-1 and ASC speck formation assays. To identify differences between these cells, we performed single-cell RNA sequencing (scRNAseq) analysis. This analysis was also used to reveal whether KIPyV and MCPyV VLPs induce different cell activation states since we observed different cell activation levels according to inflammatory cytokines' production.

ScRNAseq Reveals an Overall Conserved Gene Expression Response to PyV-Derived VLPs

In vitro differentiated THP-1 macrophages were subjected to stimulation by VLPs of KIPyV or MCPyV (and unstimulated control—PBS) for 15 h followed by single-cell RNAseq

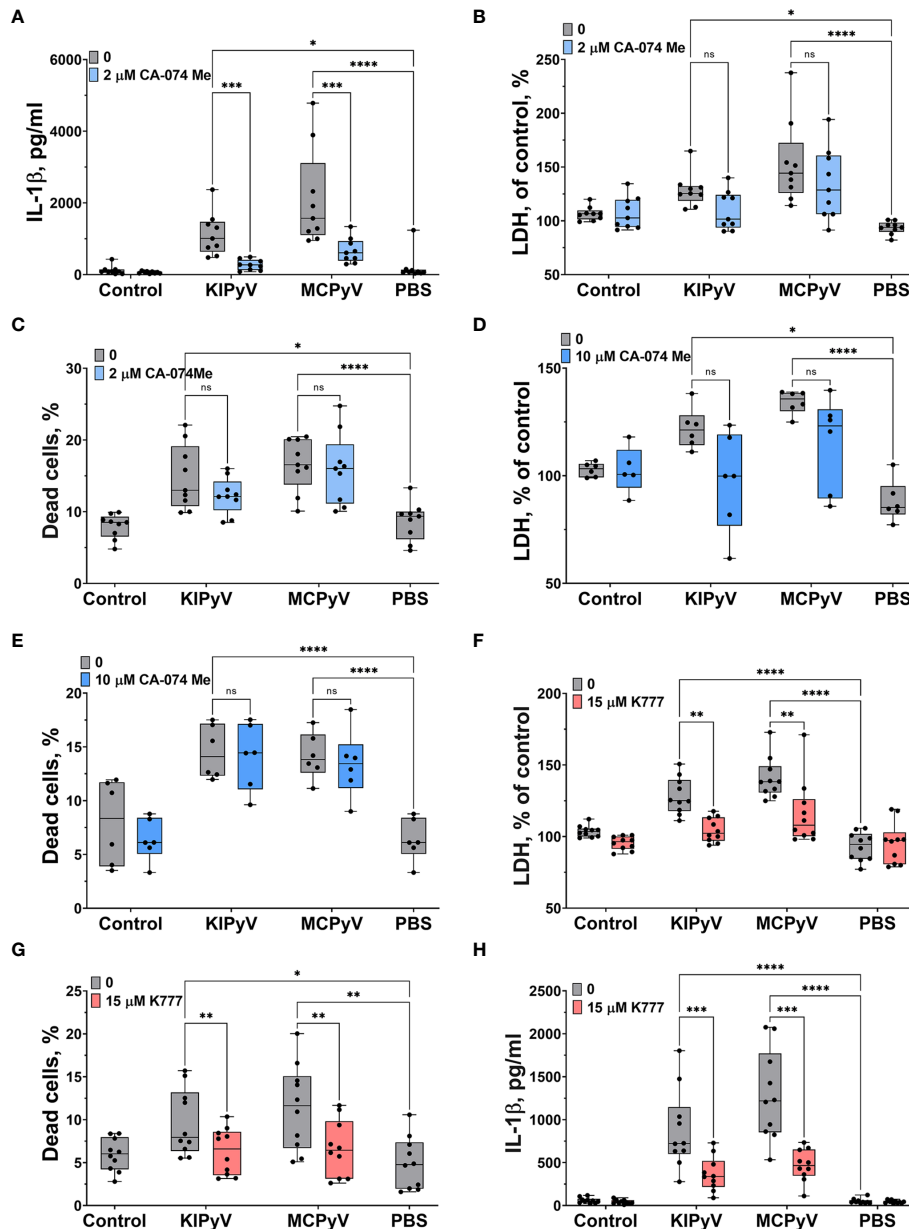


FIGURE 5 | Cathepsin B inhibitor reduced VLP-induced IL-1 β release while pan-cathepsin inhibitor decreased both IL-1 β release and cell death in human THP-1 macrophages. Macrophages were treated with PyV-derived VLPs (20 μ g/ml) for 24 h. Inhibitors CA-074 Me (2 or 10 μ M) and K777 (15 μ M) were added 30 min before treatment. **(A, H)** IL-1 β secretion by ELISA. Cytotoxicity assessed by **(B, D, F)** LDH assay and **(C, E, G)** PI and Hoechst nuclear staining. PI indicates dead cells (red) and Hoechst stains all cell nuclei (blue). Data are represented using box plots with dots showing independent experiments, * $p < 0.05$, ** $p < 0.01$, *** $p < 0.001$, **** $p < 0.0001$, one-way ANOVA followed by Tukey's multiple comparison test; ns, not statistically significant.

(Figure 8A). Upon removing transcriptomes with <900 total counts, 32,415 cells were retained, with >10,000 cells per condition. The mitochondrial gene count filter, conventionally used as a signature of dead cells (48), was omitted to enable a comparison of the viability observed from scRNAseq data.

Uniform Manifold Approximation and Projection (UMAP) visualization of scRNAseq data revealed an overall similar population structure between KIPyV and MCPyV VLP-treated

cells, and an apparent difference compared to the unstimulated control (Figure 8B). A bulk-like DGE analysis identified 43 upregulated and 12 downregulated genes in KIPyV VLP case vs. the control (Figure 8C and Supplementary Table 1). The equivalent analysis of MCPyV VLP case vs. control revealed 39 and 27 genes, respectively. By contrast, a total of 5 differentially expressed genes (DEGs) were identified when comparing MCPyV vs. KIPyV VLP-treated cells. Most of the enriched

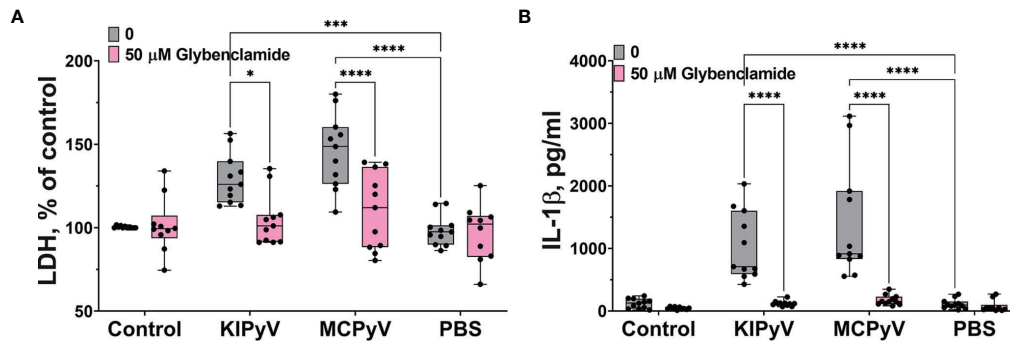


FIGURE 6 | K^+ ion efflux inhibitor reduced PyV VLP-induced cell death and IL-1 β release in human THP-1 macrophages. Macrophages were treated with PyV-derived VLPs (20 μ g/ml) for 24 h. Inhibitor glybenclamide (50 μ M) was added 30 min before treatment. **(A)** Cytotoxicity assessed by LDH assay. **(B)** IL-1 β secretion determined by ELISA. Data are represented using box plots with dots showing independent experiments, * $p < 0.05$, *** $p < 0.001$, **** $p < 0.0001$, one-way ANOVA followed by Tukey's multiple comparison test.

genes compared to the control were the same regardless of the VLPs used for stimulation, and the 5 most enriched terms in a GO gene set enrichment analysis of these common genes were associated with immune cell activation processes (migration, chemotaxis, response to TNF, and IL-1) (Figure 8D and Supplementary Figure 4, Supplementary Table 2).

ScRNAseq Reveals Multiple Subpopulations of THP-1 Macrophages and Changes in Their Abundance Upon VLP Stimulation

The UMAP visualization of scRNAseq data revealed a continuous structure with no clear boundaries between gene expression states. Upon interactive exploration (49) of gene expression patterns and Leiden clustering results at different resolution (i.e., different number of clusters), we chose to report on 9 populations (Figure 9A) of variable abundance across the 3 conditions (Figures 9B, C). For each cell population, we identified the 20 most enriched genes (FDR < 0.05, Mann-Whitney U test). Hierarchical clustering of the expression of these genes across all 9 populations revealed both distinct and overlapping gene expression signatures and the transcriptional relationship between populations (Figures 9D, E). The major split of the population dendrogram (Figure 9D) separates activated states (AI, AII, HA, and IR) enriched after VLP stimulation (Figure 9F) from SS, RS, MA, and PA. The population of dead cells cluster with the latter but form a distant branch. Consistently with cell viability assays (Figures 2D, E), the fraction of dead cells, characterized by a high expression of mitochondrial genes (Figure 9E and Supplementary Figure 5A; Supplementary Table 3), increases with VLP stimulation from 2% to 5%–6% (Figure 9C).

None of the states was completely quiescent, i.e., with all cells in the G0 stage, as suggested by a classification into cell cycle stages based on gene expression, although different populations showed a variable fraction of cells in G1/M/G2/S stages (Figure 9F).

The cell cluster most uniformly represented across the three conditions (PBS, KIPyV, and MCPyV VLPs) was called steady

state (SS) (Figures 9A, F). Among its enriched genes are *CD52*, *LMO4*, *CHI3L1*, and *COX5B* (Figure 9E and Supplementary Figure 5B; Table S3). The function of most of the proteins encoded by these genes is unclear. CD52 is a glycoprotein of an unknown function. A recent study showed the ability of soluble CD52 to suppress inflammatory cytokine production by inhibiting TLR-induced NF- κ B activation in macrophages and dendritic cells (50). *COX5B* encodes the 5B subunit of Cytochrome C Oxidase, an essential mitochondrial respiratory chain enzyme (51). An increased expression of *COX5B* may be related to an increased cellular respiration. *LMO4*-encoded protein may play a role as an oncogene targeting the TGF- β signaling pathway (52). Overall, the phenotype of SS population is unclear as the functions of most enriched genes in macrophages are unknown. In addition, GO enrichment analysis did not show any relation to known GO terms (Figure 9E). Therefore, this population could be described as a new possible phenotype of the THP-1 cell line.

One cell cluster, the relative abundance of which changed upon cell activation, was called resting state (RS) (Figure 9A). This cell population did not express inflammatory molecules, and the enriched genes were related to usual cellular processes. Even so, this cluster distinguished oneself by high enrichment of *ARHGAP18*, *TMEM158*, *TGM2*, *OXR*, and *FN1*, which have vital or still unknown functions (Figure 9E and Supplementary Figure 5C; Supplementary Table 3). *ARHGAP18* encodes Rho GTPase Activating Protein 18, which is essential for actin remodeling; thus, it is important for cell migration and controls cell shape (53). *TMEM158* encodes Transmembrane Protein 158, whose biological function is unclear, although its involvement in the activation of Ras pathway was shown. It was reported that *TMEM158* enhanced proliferation and migration of cancer cells (54, 55). For example, another transmembrane protein, *TMEM119*, was identified as a marker of microglia, representing microglia with homeostatic properties (56, 57). Noticeably, *TMEM158* expression decreased after activation with VLPs addressing its presence in ramified macrophages (Supplementary Figure 5I). *TGM2* encodes Transglutaminase 2 implicated in cell death pathways (58).

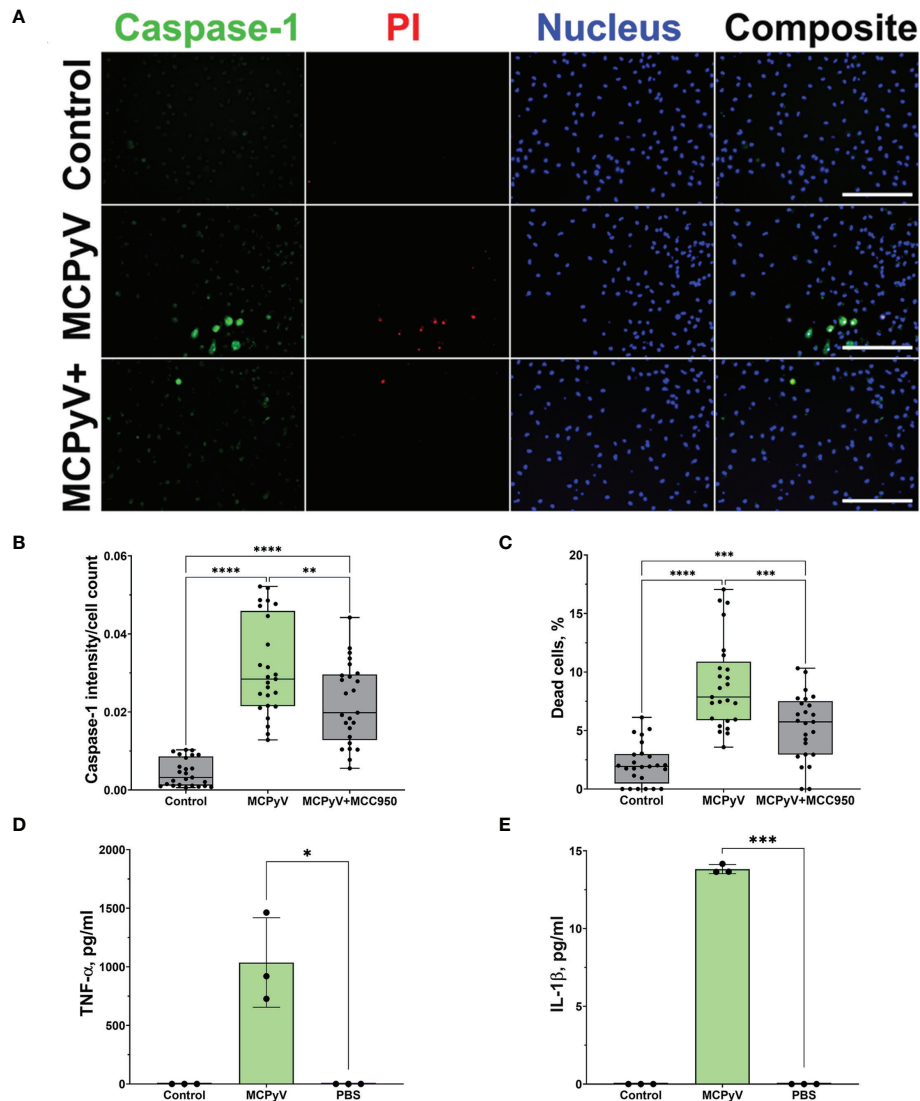


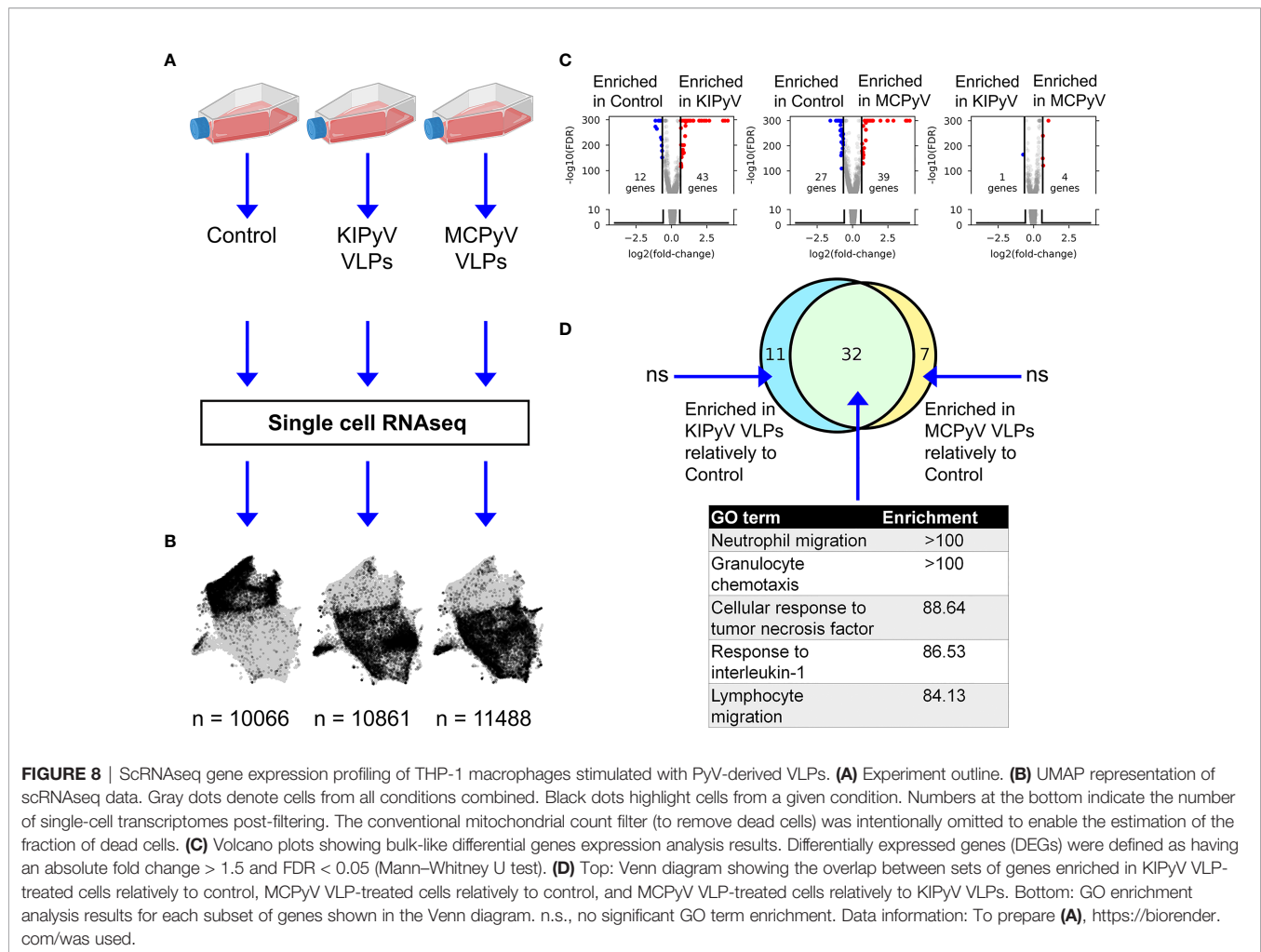
FIGURE 7 | PyV-derived VLPs activated NLRP3 inflammasome in primary human macrophages-derived from peripheral blood mononuclear cells. Macrophages were treated for 15 h with PyV-derived VLPs (20 $\mu\text{g}/\text{ml}$); inhibitor MCC950 (1 μM) was added 30 min before treatment. **(A)** Cells were stained for activated caspase-1 using FLICA (green), dead cell nuclear stain PI (red), and nuclear stain Hoechst (blue). The images were taken using 20 \times objective. Representative images of the staining are shown. The scale bars indicate 100 μm . **(B)** Quantification of dead cells, $n = 25$ photos per condition. **(C)** Caspase-1 quantification according to FLICA analysis, $n = 25$ photos per condition. After 24 h treatment with PyV-derived VLPs, collected supernatants were analyzed by ELISA for **(D)** TNF- α and **(E)** IL-1 β release, $n = 3$ technical repeats. For **(A–C)**, data were analyzed using one-way ANOVA followed by Tukey's multiple comparison test and represented using box plots with dots showing individual data points. For **(D, E)** Student's t -test was used and data were represented using bar graphs (means \pm SD) with dots showing individual data points. * $p < 0.05$, ** $p < 0.01$, *** $p < 0.001$, **** $p < 0.0001$. $N = 1$.

OXR1 encodes Oxidation Resistance Protein 1, which is involved in protection from oxidative stress and is important for lysosomal function (59, 60). *FNI* encodes fibronectin 1 known for its function in cell adhesion, motility, and maintenance of cell shape (61, 62). Therefore, expression of these genes indicates restful cells.

Another cell cluster that changed upon cell activation was called metabolically active (MA) (Figure 9A). It had a higher expression of mitochondrial and ribosomal genes, for example, *MT-CO3*, *MT-CYB*, *RPL37A*, and *RPS23* (Figure 9E and Supplementary Figure 5D). The MA cluster did not show

expression of genes related to inflammatory cell activation, but the observed gene expression profile indicates increased cellular respiration that is related to high cell metabolic activity (63). Enrichment in ribosomal genes characterized protein production indicating metabolic cell activity.

In the control condition (PBS) we found a cluster in which the cells seemed to be activated *a priori*. It was named prone to activation (PA) (Figure 9A). Higher expression of *SPPI*, *CTSC*, *TREM2*, *S100A4*, and *IL1B* was detected in some cells of this cluster (Figure 9E; Supplementary Figure 5E and



Supplementary Table 3). It is possible that these cells showed a delayed response to phorbol 12-myristate 13-acetate (PMA) used for THP-1 differentiation. This cell cluster disappeared after treatment with VLPs. *CTSC* encodes lysosomal protease Cathepsin C. As other cathepsins, *CTSC* is important for cargo degradation (64). *CTSC* was also shown to be necessary for activating serine proteases since its absence altered extracellular IL-1 β activation (65). In addition, upregulation of *CTSC* mediates macrophage polarization to inflammatory phenotype (66, 67). *S100A4* encodes calcium-binding protein *S100A4* involved in inflammatory reactions (68, 69). *SPP1* encodes Secreted Phosphoprotein 1 that is chemotactic, induces IFN- γ and IL-12 production, and promotes cell survival (70). *TREM2* encodes Triggering Receptor Expressed on Myeloid Cells 2 that triggers secretion of inflammatory molecules (71, 72), although the anti-inflammatory effect of *TREM2* was demonstrated in macrophages lacking *TREM2* as toll-like receptor stimulation induced higher pro-inflammatory cytokine secretion (73). Soluble *TREM2* was identified as an activator of inflammatory response (74). It enhances phagocytosis as its loss impairs cellular uptake of various substrates, such as cellular debris (75), bacteria (76), or amyloid-beta aggregates (77). Overall, PA cells are differently

activated compared to other THP-1 cell populations (AI, AII, HA, and IF), and they distinguish themselves as having inflammation-related and phagocytic cell properties.

The cluster of cells formed upon VLP stimulation was defined as a high activation (HA) state (**Figure 9A**). This cluster was more abundant in MCPyV VLP-treated cells than in KIPyV VLP-treated cells (**Figure 9F**). This cell population was characterized with the highest expression of *IL1B* and chemokine genes, such as *CXCL1*, *CXCL3*, *CXCL8*, *CCL3*, *CCL20*, *CCL4L2*, and *CSTB* (**Figure 9E** and **Supplementary Figure 5G**; **Supplementary Table 3**). It is known that *IL1B* is expressed at extremely high levels in myeloid-derived cells in response to microbial invasion and tissue injury (78). The product of *IL1B* is pro-inflammatory cytokine IL-1 β , a key mediator of inflammation and one of the main indicators of NLRP3 inflammasome assembly (79). IL-1 β induces the production of chemokines and proteases to attract other immune cells to the infection site. Furthermore, secretion of chemokines is reduced in NLRP3-deficient mice demonstrating the importance of inflammasome activation in chemotaxis (80). IL-1 β is a product of inflammasome activation; thus, factors stimulating the inflammasome also recruit immune cells.

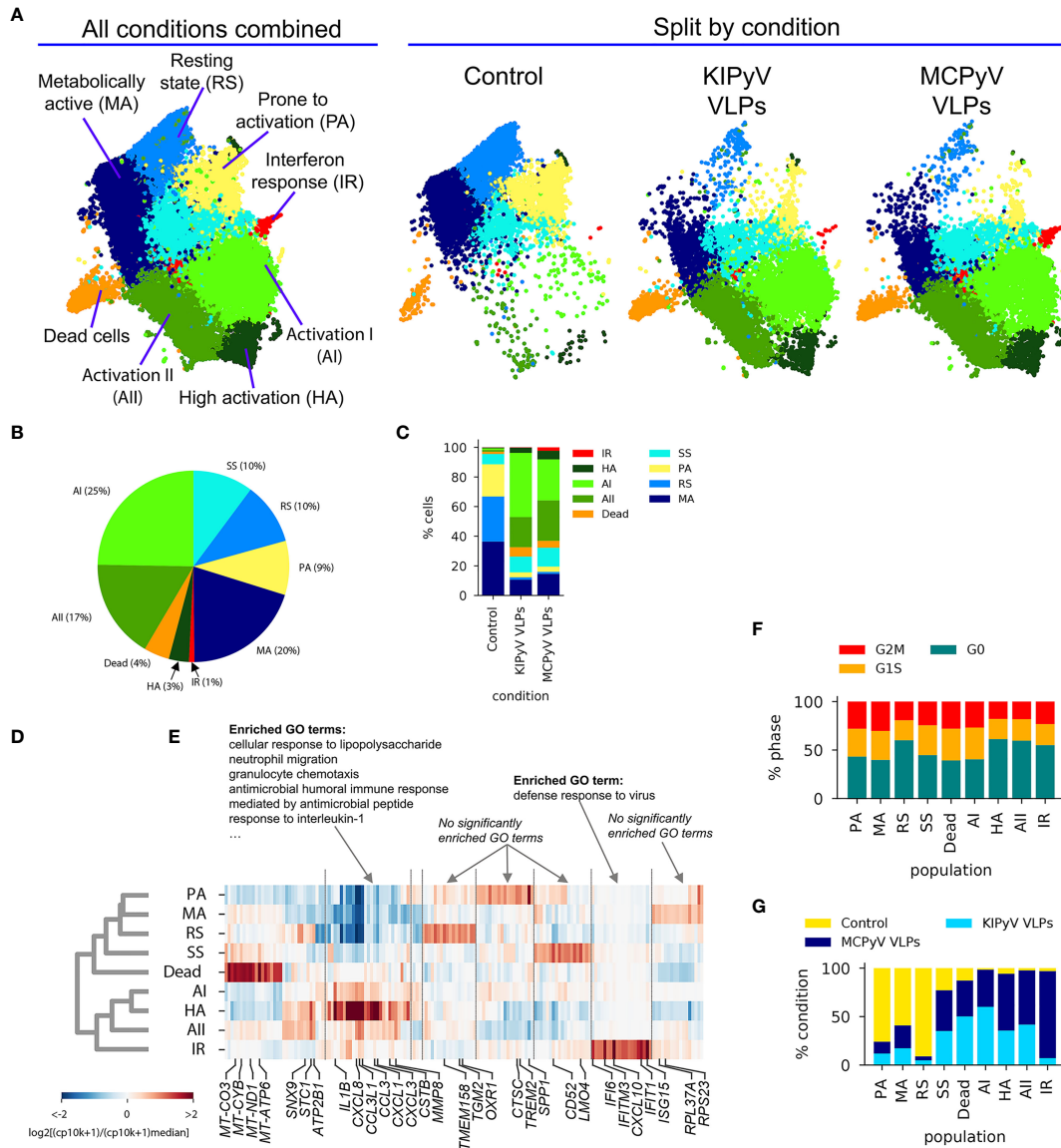
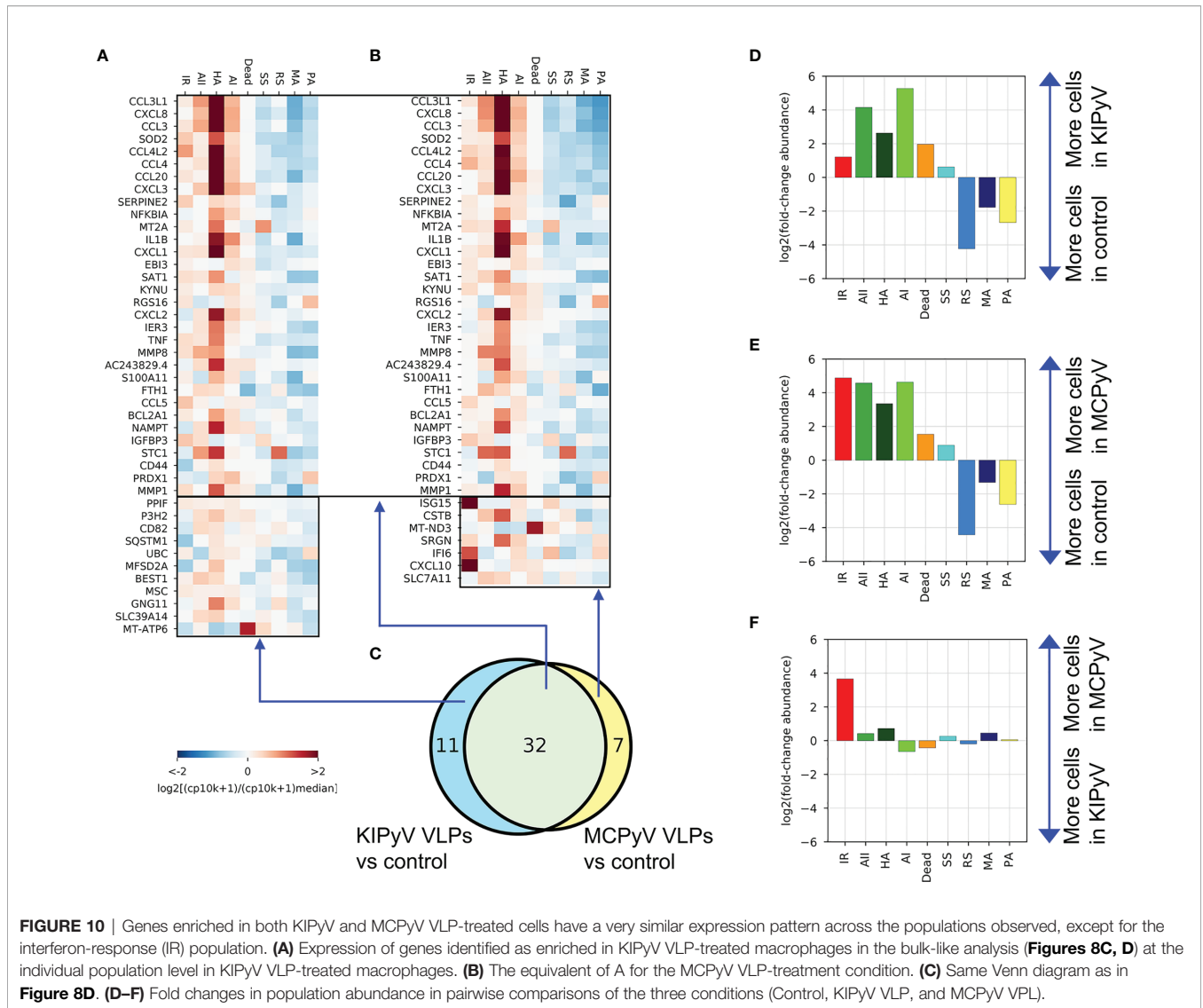


FIGURE 9 | ScRNAseq revealed different cell populations within THP-1 macrophages treated with PyV-derived VLPs. **(A)** UMAP colored by cell population annotation either combining all conditions (left) or split by condition (right). Percentages of cells per population for all data combined **(B)** or split by condition **(C)**. Results of population-enriched gene identification, including a population dendrogram **(D)** based on hierarchical clustering (correlation distance measure, average linkage) by enriched gene expression **(E)**. Selected genes are highlighted at the bottom. Results of GO enrichment analysis on selected genes groups are shown on top. CP10K—counts per 10,000. **(F)** Relative abundances of each population by condition. As this analysis is sensitive to the total number of cells sampled by condition, cell counts from each condition were first normalized to 10,000. **(G)** Relative abundance of cells at different cell cycle stages defined based on gene expression scoring.

CXCL1, *CXCL3*, and *CXCL8* encode members of the CXC subfamily of chemokines, the chemoattractants for neutrophils (81). *CXCL8*, also known as IL-8, has no homologs in rats or mice and is a significant component of inflammation-mediated processes as it attracts neutrophils, basophils, and T cells to the site of infection and promotes endothelial cell migration and proliferation (82). HA state is also rich in genes of other chemoattractants *CCL3* and *CCL20*. *CCL3*, also known as macrophage inflammatory protein 1 alpha, is induced by NF-

κB signaling pathway and triggers inflammatory reactions (83). *CCL20* acts as a ligand for C-C chemokine receptor *CCR6* that induces a strong chemotactic response and plays an important role at skin and mucosal surfaces under homeostatic and inflammatory conditions (84). HA cluster was also highly enriched in *CSTB*, which encodes cystatin B, a cysteine protease inhibitor known to interact with cathepsin B (85) and considered to protect from cathepsin leakage from damaged lysosomes (86). *CSTB* expression reveals possible lysosomal damage induced by



VLPs. Overall, highly enriched genes of HA state showed a strong inflammatory response in VLP-treated macrophages.

Other cell clusters formed upon cell activation were named the Activation I (AI) and Activation II (AII) states (**Figure 9A**). AI cluster was more characteristic for KIPyV than MCPyV VLP-treated cells and AII state, and *vice versa* (**Figure 9F**). Both clusters had enriched inflammation-related genes similarly to HA state but at lower levels (**Figure 9E**). AI state was characterized by high *IL1B*, *CXCL8*, *CCL3L1*, and *CCL3* expression (**Figure 9E** and **Supplementary Figure 5F**; **Supplementary Table 3**). AII had relatively low expression of *IL1B* but the enrichment in *CXCL8*, *CCL3L1*, and *CCL3* was similar to AI. In general, the same genes were enriched in HA, AI, and AII states, although the expression levels were different. Furthermore, HA and AII were different from AI state as HA and AII had enrichment in *STC1*, *MMP8*, *ATP2B1*, *FTH1*, and *SNX9* genes. Interestingly, enrichment in some of these genes, like *ATP2B1* and *SNX9*, was similar to RS cluster. *STC1* is known to encode Stanniocalcin 1, a secreted glycoprotein involved in inflammation

and carcinogenesis (87) that possibly serves as a negative mediator of inflammation (88). Interestingly, HA state, which was highly enriched in pro-inflammatory cytokines, also expressed high levels of *STC1*. *MMP8* is a Matrix Metalloproteinase-8 that cleaves collagen, some cell adhesion proteins, growth factors, and chemokines (89), and promotes polarization of macrophages into alternatively activated (M2) macrophages (90). Therefore, AII and HA states describe a group of activated macrophages expressing inflammation-related genes and a couple of inflammation suppressors. *SNX9* encodes Sorting Nexin 9 involved in intracellular trafficking (91) and regulates clathrin-mediated endocytosis (92). It also plays a role in inflammatory reactions (93) and regulation of the micropinocytosis–endocytosis pathway (94). In innate immune cells, this endocytosis pathway may function for the delivery of antigens to their respective intracellular pattern recognition receptors (95). Since the endocytosis pathway of polyomavirus VLPs is unclear, *SNX9* may contribute to intracellular recognition of VLPs. *ATP2B1* encodes Plasma Membrane Calcium ATPase 1

(PMCA1) important in maintaining cytosolic Ca^{2+} for physiological cell functions (96). Ca^{2+} mobilization is critical for NLRP3 inflammasome activation (97). Thus, calcium pumps could be implicated in inflammasome signaling detected after VLP treatment. *FTH1* encodes the heavy subunit of ferritin, which is essential to store iron inside cells (98). Macrophages are central players in iron metabolism as they recycle senescent erythrocytes and modulate iron availability as part of host protective mechanisms (99). *FTH1* is crucial in protection against iron-induced oxidative stress (100). In summary, HA and AI clusters next to inflammation-related genes also expressed higher levels of genes encoding ion channels and proteins involved in endocytosis contrary to AI state.

While Most Population and Gene Expression Changes Are Conserved, Interferon-Response Population Is Highly Enriched Upon Activation With MCPyV-Derived VLPs

Analysis of the previously identified (Figures 8C, D) global gene expression changes at the individual population level revealed very similar gene expression patterns between KIPyV and MCPyV VLP-treated THP-1 cells (Figures 10A–C and Supplementary Figure 6A). A population abundance fold-change analysis emphasized the overall similar phenotype of the two VLP-treatment conditions (Figure 10F), while differences in abundance relatively to control exceeded 30× (Figures 10D, E). However, a notable exception was the interferon-response population (IR), highly enriched after MCPyV VLP stimulation compared to KIPyV VLP and absent in control cells (Figures 10D, E and Supplementary Figure 6B). This suggests differences in pathogen-associated molecular patterns derived from human PyVs. IR population was characterized by the expression of *CXCL10*, *ISG15*, *IFITM3*, *IFIT1-3*, *IFI6*, *CXCL11*, and other genes (Figure 9E and Supplementary Figure 5H; Supplementary Table 3), known to be involved in inhibition of viral invasion. We assume that macrophage engagement with viral antigens itself mediates antiviral activity in macrophages without external stimulation, such as lipopolysaccharide.

In detail, most of IR cluster genes are induced by interferon (IFN) and related to cell response during viral infection. *IFITMs* encode Interferon-Induced Transmembrane Proteins that limit viral infection *via* entry pathway (101). In interferon-stimulated cells, *IFITM3* is localized on endocytic vesicles that fuse with incoming virus particles and enhance their trafficking to lysosomes (102). A recent study revealed that *IFITM3* is able to inhibit SARS-CoV-2 infection *in vitro* (103). *IFITs* encode Interferon-Induced Proteins with Tetratricopeptide repeats that block viral infection by interacting with factors responsible for virus replication (104). *IFI6* encodes Interferon- α Inducible Protein 6. The exact function of this protein is still unclear. The family of *IFI6* genes encodes mitochondrial proteins implicated in inhibition of apoptosis (105). *IFI6* was also shown to inhibit DNA replication in hepatitis B virus (106). *ISG15* (Interferon Stimulated Gene 15) encodes ubiquitin-like protein that is induced by type I interferons and involved in

various processes related to host antiviral response (107). Its upregulation was detected in macrophages after infection by vaccinia and SARS-CoV-2 viruses (108, 109). This protein is likely to be an important factor implicated in cytokine storms triggered by SARS-CoV-2. *ISG15* deletion in bone marrow-derived macrophages induced mitochondrial dysfunction and altered nitric oxide production exposing its importance in regulating mitochondrial function (110). Other genes rich in IR state encode *CXCL10* and *CXCL11*, but the latter expression was detected only in several cells. *CXCL10* is known as early interferon response gene encoding *CXCL10* with inflammation-related pleiotropic effects (111). *CXCL11* participates in inflammatory reactions and acts as a chemoattractant of activated T cells (112). *CXCL10* and *CXCL11* are thought to be key mediators of the cytokine storm in immune response to SARS-CoV-2 infection (113). Overall, high expression of IR-specific genes indicates cellular response to interferon induced in THP-1 cells by VLP treatment.

DISCUSSION

In our study, we focused on the inflammatory response of human macrophages treated with viral oligomeric proteins. Cellular response to nanoparticles has been explored previously, covering different mechanisms. It was demonstrated that polymeric nanoparticles induced NLRP3 inflammasome activation dependent on cathepsin B in macrophages (114). Another study showed that oligomeric proteins, A β fibrils, cause lysosomal damage and induce inflammasome activation (115). In addition, tau oligomers and α -synuclein fibrils were shown to trigger an inflammatory response in microglia (11, 116). The latter reports demonstrated inflammasome activation in macrophages by endogenous pathogenic protein oligomers. However, there are limited data on molecular mechanisms and how oligomeric proteins activate NLRP3 inflammasome. To address this question, we investigated the ability of exogenous oligomeric proteins of viral origin to induce inflammatory responses in human macrophages.

In our study, we have used different viral oligomeric proteins—filamentous NLPs of measles and mumps viruses and spherical VLPs of KIPyV and MCPyV. We did not observe any inflammatory response to NLPs, although NLRP3 inflammasome activation was demonstrated to be induced by N protein of SARS-CoV-2 (117). Interestingly, N protein of SARS-CoV-2 inhibits the cleavage of gasdermin D, which forms pores in the membrane, reducing IL-1 β secretion and pyroptosis (118). In our study, only PyV-derived VLPs induced inflammatory response of human macrophages followed by NLRP3 inflammasome activation. Specific NLRP3 inflammasome inhibitor MCC950 blocked the detected activation signal proving that PyV-derived VLPs are a trigger of NLRP3 inflammasome. In addition, VLPs induced secretion of other inflammatory cytokines TNF- α and IL-6, suggesting the engagement of NF- κ B signaling pathway in the activated macrophages.

NLRP3 inflammasome can be activated by different mechanisms, such as changes in intracellular ion concentration,

mitochondrial, or lysosomal damage followed by cathepsins release (119). First, we studied inflammasome activation mechanism related to lysosomal damage since PyV-derived VLPs are phagocytosed particles. The VLP-induced inflammasome activation signal was significantly reduced by cathepsin B and pan-cathepsin inhibitors. However, the inhibitory effect was not complete compared to control. Cathepsin B inhibitor reduced only IL-1 β release and had no effect on cell death. In the case of MCPyV-derived VLPs, IL-1 β secretion and cell death did not drop to control baseline even using pan-cathepsin inhibitor. In the case of KIPyV-derived VLPs, pan-cathepsin inhibitor completely reduced cell death, contrary to IL-1 β release. This suggests that VLP size and possibly other structural features of VLPs may define cell activation profile. Viral capsids of KIPyV and MCPyV are structurally different; thus, they may interact with different cellular receptors. In addition, the hemagglutination ability was demonstrated only for MCPyV, indicating different glycoproteins on KIPyV and MCPyV capsid surface (120, 121).

There are controversial data on particle-induced inflammasome activation. Some of them show that nanoparticles induce NLRP3 inflammasome activation *via* phagosomal destabilization (122). Other studies reveal that different nanoparticles induce different mechanisms depending on the composition and structure of the particles (123). For example, cholesterol crystals activate NLRP3 inflammasome; however, inhibitors of cathepsins reduce only IL-1 β release and do not change the level of cell death. The role of cathepsins in inflammasome activation is not fully understood. It was recently shown that cathepsins can induce activation of pore-forming protein gasdermin D (124). We assumed that PyV-derived VLPs induced inflammasome activation *via* lysosomal damage and investigated the underlying mechanisms, in particular the mechanism of K⁺ ion efflux. We demonstrated that a specific inhibitor of K⁺ ion efflux significantly reduced cell death and IL-1 β release, suggesting the complexity of macrophage activation by PyV-derived VLPs. In addition, studies on the possible outcome of lysosomal leakage indicate that effector molecules such as cathepsins released after the permeabilization of lysosomal membrane may activate the inflammasome by several mechanisms, including K⁺ ion efflux and intracellular Ca²⁺-initiated signaling events (125). Cathepsins can also induce synthesis of IL-1 β precursor, leading to a higher release of inflammatory cytokines and involvement of cathepsins in NF- κ B signaling (126). This demonstrates that inflammasome activation by phagocytosed particles is beyond the classical mechanism.

Moreover, we have observed a different pattern of cell activation by VLPs and nigericin—a small molecule that promotes K⁺ efflux and activates NLRP3 inflammasome. In contrast to nigericin that induced caspase-1 expression and ASC speck formation within the first hours of treatment, VLPs induced the formation of ASC specks after 15 h of treatment. These findings might be explained by the fact that nigericin makes pores in cell membranes finally leading to cell lysis, while VLPs induce inflammasome activation *via* a phagocytosis-related pathway.

Finally, we proved the inflammatory response observed in human macrophage cell line THP-1 to PyV-derived VLPs using

primary human macrophages. The same cellular events were identified in both the THP-1 cell line and the primary human macrophages. Activated caspase-1 was detected in dead primary macrophages, suggesting the pyroptotic cell death. As in THP-1 experiments, only a part of the primary macrophages was activated by the VLPs. Thus, large-sized multimeric protein particles, VLPs, are capable of inducing a similar cell activation pattern in both macrophage cell line and primary human macrophages.

From *in vitro* studies, it is well known that strong inducers of inflammation, such as lipopolysaccharides, can induce high cell activation states. However, other cell activators usually mediate modest cellular response. For example, in previous research, we showed lower inflammasome activation by A β oligomers compared to the classical NLRP3 inflammasome inducer nigericin (9). However, when A β -activated cells were observed microscopically, it was clear that not all of them exhibited similar level of inflammasome activation. It raises a question on the activation state of separate cells. The presence of heterogeneous cell populations was demonstrated several times by other groups. For example, microglia are at different cell activation states depending on the distance from amyloid-beta (A β) plaque in the brain of Alzheimer's disease patients (127). In addition, microglia are heterogeneous in healthy brain, and cells enriched in inflammation-related genes are present throughout the lifespan and increase in the aged brain (128). ScRNAseq analysis of peripheral blood mononuclear cell culture revealed that monocytes respond differently to lipopolysaccharide (129). One cell population expressed pro-inflammatory alarmins and chemokines to attract immune cells while another was enriched in later inflammation-related and anti-inflammatory genes to either enhance or terminate inflammatory reaction. In our study, IL-1 β and TNF- α release data showed overall cell activation by PyV-derived VLPs; however, caspase-1, ASC speck, and cell viability assays allowed the identification of differently activated cells. Therefore, we performed a single-cell analysis to identify gene expression differences in cells, which primarily were expected to be homogeneous—THP-1 cell culture model.

ScRNAseq analysis showed a highly divergent cell activation pattern after treatment with PyV-derived VLPs. Four activated THP-1 cell populations varying in expression of inflammation-related genes, among them IL1B and chemokine genes, were identified. IL-1 family cytokines are known to induce the production of chemokines (130). The stress response and prolonged inflammation also lead to recruitment of immune cells (131). Therefore, increased chemokine expression in cells, enriched in IL-1 β and other inflammation mediators, indicates a strong inflammatory response. After VLP treatment, one cell cluster was highly enriched in inflammation-related genes (HA state), including IL-1 β . This population was also enriched in CSTB, which encodes cystatin B, an inhibitor of cathepsin B. It possibly copes with cathepsins released after lysosomal leakage (86). Therefore, CSTB expression verifies lysosomal damage induced by VLPs. This cell cluster may represent a population of inflammasome-activated cells, which we revealed according to ASC speck formation, cell viability, and caspase-1 assays.

Interestingly, two populations of activated cells, including the HA cell cluster, also expressed negative mediators of inflammation next to inflammation-related genes. This may indicate a prolonged cell activation state when self-protecting genes were switched on to avoid hyperinflammation. It is known that inflammatory response follows the resolution phase when anti-inflammatory molecules are secreted (132).

Comparing KIPyV and MCPyV VLP-induced cellular response, we found higher expression of interferon response-related genes after MCPyV VLP treatment. This extends the known differences of KIPyV and MCPyV VLPs. Among interferon-response genes were CXCL10 and IGS15, involved in host antiviral response and found to induce cytokine storm in SARS-CoV-2-infected patients (108, 113). Interferon-induced proteins participate in inflammatory reactions and attract different cells of innate and adaptive immunity. Interferon-stimulated genes can be triggered not only by viral antigens directly but also by cellular stress response; thus, their encoded proteins may have a broader biological function (133).

Summarizing, single-cell analysis revealed the presence of heterogeneous cell populations in the *in vitro* cell culture model, THP-1 macrophages, which might be expected to be a homogeneous cell culture. Although the molecular mechanisms behind different cell activation states are unknown, our study shows that some cells respond to the activating agent by inflammatory reactions while other cells remain unaffected. Assuming the inflammasome activation by protein oligomers as a result of phagocytosis-related process, we suppose that some cells are capable of degrading their cargo and some not, which may lead to lysosomal disruption.

Next to the inflammasome, several other mechanisms are implicated in the response of immune cells to intact viruses or viral components. One example is toll-like receptors (TLRs), such as TLR2 and TLR4, which recognize a variety of microbial molecules, among them viral proteins (134). After TLR activation, NF- κ B signaling cascade is initiated to induce expression of pro-inflammatory cytokines. It was demonstrated that polyomavirus VP1 pentamers bind to TLR2 on antigen-presenting cells and induce IL-12 secretion (135). In addition, our results show that PyV-derived VLPs induced NF- κ B activation. Interestingly, TLR2 activation is also induced by α -synuclein oligomers (136). TLR activation by human papillomavirus-derived VLPs leading to production of pro-inflammatory cytokines was also demonstrated (137, 138). Therefore, VLPs may trigger TLR2-mediated NF- κ B activation, followed by pro-inflammatory cytokine production. Similar processes were induced by surface glycoproteins of other viruses, for example, gH/gL and gB of herpes simplex virus (139, 140), and gB and gH of human cytomegalovirus (141). Non-structural viral proteins were also demonstrated to activate TLRs. Non-structural protein 1 (NS1) of dengue virus activated TLR4 (142) while both NS3 and capsid proteins of hepatitis C virus activated TLR2, inducing pro-inflammatory cytokine release (143). NLRP3 inflammasome activation in macrophages by hepatitis C capsid protein was also demonstrated (144),

suggesting that the same viral protein can mediate several cell signaling cascades.

Inactivated viruses and recombinant viral proteins are broadly used for vaccination (145). However, the mechanisms of the immune response and especially activation of the innate immunity components induced by viral proteins are barely investigated. Therefore, the results of our study on PyV-derived VLPs as potent inducers of the inflammatory response in macrophages as compared to filamentous NLPs that are incapable to trigger the inflammation would broaden the understanding of the interaction of viral proteins with innate immune cells. Our study suggests that not all viral proteins can trigger the inflammatory response depending on the structural properties.

DATA AVAILABILITY STATEMENT

The original contributions presented in the study are publicly available. This data can be found here: <https://www.ncbi.nlm.nih.gov/geo/query/acc.cgi?acc=GSE190666>.

AUTHOR CONTRIBUTIONS

AL designed experiments, analyzed the data, and wrote the manuscript. ID and KM contributed to the experiments and manuscript writing. MN was responsible for VLP preparation. AŠ performed single-cell RNA sequencing. RŽ was responsible for single-cell RNA sequencing analysis. IK-K and AG helped to design the experiments and were responsible for manuscript revision. AŽ was responsible for the final manuscript revision. All authors contributed to the article and approved the submitted version.

FUNDING

This study was supported by the Research Council of Lithuania, grant No. S-SEN-20-11.

ACKNOWLEDGMENTS

We would like to thank Prof. L. Mažutis for cell line THP-1.

SUPPLEMENTARY MATERIAL

The Supplementary Material for this article can be found online at: <https://www.frontiersin.org/articles/10.3389/fimmu.2022.831815/full#supplementary-material>

REFERENCES

- Oishi Y, Manabe I. Macrophages in Age-Related Chronic Inflammatory Diseases. *NPJ Aging Mech Dis* (2016) 2:8. doi: 10.1038/npjamd.2016.18
- Parisi L, Gini E, Baci D, Tremolati M, Fanuli M, Bassani B, et al. Macrophage Polarization in Chronic Inflammatory Diseases: Killers or Builders? *J Immunol Res* (2018) 2018:8917804. doi: 10.1155/2018/8917804
- Zhang C, Yang M, Ericsson AC. Function of Macrophages in Disease: Current Understanding on Molecular Mechanisms. *Front Immunol* (2021) 12:620510. doi: 10.3389/fimmu.2021.620510
- Shu F, Shi Y. Systematic Overview of Solid Particles and Their Host Responses. *Front Immunol* (2018) 9:1157. doi: 10.3389/fimmu.2018.01157
- Rabollí V, Lison D, Huaux F. The Complex Cascade of Cellular Events Governing Inflammasome Activation and IL-1 Beta Processing in Response to Inhaled Particles. *Particle Fibre Toxicol* (2016) 13:17. doi: 10.1186/s12989-016-0150-8
- de Alba E. Structure, Interactions and Self-Assembly of ASC-Dependent Inflammasomes. *Arch Biochem Biophys* (2019) 670:15–31. doi: 10.1016/j.abb.2019.05.023
- Swanson KV, Deng M, Ting JP. The NLRP3 Inflammasome: Molecular Activation and Regulation to Therapeutics. *Nat Rev Immunol* (2019) 19 (8):477–89. doi: 10.1038/s41577-019-0165-0
- Fusco R, Siracusa R, Genovese T, Cuzzocrea S, Di Paola R. Focus on the Role of NLRP3 Inflammasome in Diseases. *Int J Mol Sci* (2020) 21(12):4223. doi: 10.3390/ijms21124223
- Luciūnaitė A, McManus RM, Jankunec M, Raczy I, Dansokho C, Dalgediene I, et al. Soluble A Beta Oligomers and Protofibrils Induce NLRP3 Inflammasome Activation in Microglia. *J Neurochem* (2020) 155(6):650–61. doi: 10.1111/jnc.14945
- Codolo G, Plotegher N, Pozzobon T, Brucalè M, Tessari I, Bubacco L, et al. Triggering of Inflammasome by Aggregated α -Synuclein, an Inflammatory Response in Synucleinopathies. *PLoS One* (2013) 8(1):e55375. doi: 10.1371/journal.pone.0055375
- Ising C, Venegas C, Zhang S, Scheiblich H, Schmidt SV, Vieira-Saecker A, et al. NLRP3 Inflammasome Activation Drives Tau Pathology. *Nature* (2019) 575(7784):669–73. doi: 10.1038/s41586-019-1769-z
- Doshi N, Mitragotri S. Macrophages Recognize Size and Shape of Their Targets. *PLoS One* (2010) 5(3):e10051. doi: 10.1371/journal.pone.0010051
- Samstad EO, Niyonzima N, Nymo S, Aune MH, Ryan L, Bakke SS, et al. Cholesterol Crystals Induce Complement-Dependent Inflammasome Activation and Cytokine Release. *J Immunol* (2014) 192(6):2837–45. doi: 10.4049/jimmunol.1302484
- Dostert C, Pettrilli V, Van Bruggen R, Steele C, Mossman BT, Tschopp J. Innate Immune Activation Through Nalp3 Inflammasome Sensing of Asbestos and Silica. *Science* (2008) 320(5876):674–7. doi: 10.1126/science.1156995
- Baranov MV, Kumar M, Sacanna S, Thutupalli S, van den Bogaart G. Modulation of Immune Responses by Particle Size and Shape. *Front Immunol* (2020) 11:607945. doi: 10.3389/fimmu.2020.607945
- Dalgediene I, Luciūnaitė A, Zvirbliene A. Activation of Macrophages by Oligomeric Proteins of Different Size and Origin. *Mediators Inflamm* (2018) 2018:7501985. doi: 10.1155/2018/7501985
- Wang WB, Li G, Wu D, Luo Z, Pan P, Tian MF, et al. Zika Virus Infection Induces Host Inflammatory Responses by Facilitating NLRP3 Inflammasome Assembly and Interleukin-1 Beta Secretion. *Nat Commun* (2018) 9:16. doi: 10.1038/s41467-017-02645-3
- Maloney C, Jensen S, Gil-Rivas V, Goolkasian P. Latent Viral Immune Inflammatory Response Model for Chronic Multisymptom Illness. *Med Hypotheses* (2013) 80(3):220–9. doi: 10.1016/j.mehy.2012.11.024
- De Gascun CF, Carr MJ. Human Polyomavirus Reactivation: Disease Pathogenesis and Treatment Approaches. *Clin Dev Immunol* (2013) 2013:373579. doi: 10.1155/2013/373579
- Effendi WI, Nagano T. The Crucial Role of NLRP3 Inflammasome in Viral Infection-Associated Fibrosing Interstitial Lung Diseases. *Int J Mol Sci* (2021) 22(19):10447. doi: 10.3390/ijms221910447
- Ansari MA, Singh VV, Dutta S, Veetil MV, Dutta D, Chikoti L, et al. Constitutive Interferon-Inducible Protein 16-Inflammasome Activation During Epstein-Barr Virus Latency I, II, and III in B and Epithelial Cells. *J Virol* (2013) 87(15):8606–23. doi: 10.1128/JVI.00805-13
- Singh VV, Kerur N, Bottero V, Dutta S, Chakraborty S, Ansari MA, et al. Kaposi's Sarcoma-Associated Herpesvirus Latency in Endothelial and B Cells Activates Gamma Interferon-Inducible Protein 16-Mediated Inflammasomes. *J Virol* (2013) 87(8):4417–31. doi: 10.1128/JVI.03282-12
- Li YH, Wei X, Ji S, Gui SY, Zhang SM. *In Vivo* Effects of the NLRP1/NLRP3 Inflammasome Pathway on Latent Respiratory Virus Infection. *Int J Mol Med* (2018) 41(6):3620–8. doi: 10.3892/ijmm.2018.3521
- Marcocci ME, Napoletani G, Protto V, Kolesova O, Piacentini R, Li Puma DD, et al. Herpes Simplex Virus-1 in the Brain: The Dark Side of a Sneaky Infection. *Trends Microbiol* (2020) 28(10):808–20. doi: 10.1016/j.tim.2020.03.003
- Burgos JS, Ramirez C, Sastre I, Valdivieso F. Effect of Apolipoprotein E on the Cerebral Load of Latent Herpes Simplex Virus Type 1 DNA. *J Virol* (2006) 80(11):5383–7. doi: 10.1128/JVI.00006-06
- Bourgade K, Garneau H, Giroux G, Le Page AY, Bocti C, Dupuis G, et al. β -Amyloid Peptides Display Protective Activity Against the Human Alzheimer's Disease-Associated Herpes Simplex Virus-1. *Biogerontology* (2015) 16(1):85–98. doi: 10.1007/s10522-014-9538-8
- Bourgade K, Le Page A, Bocti C, Witkowski JM, Dupuis G, Frost EH, et al. Protective Effect of Amyloid- β Peptides Against Herpes Simplex Virus-1 Infection in a Neuronal Cell Culture Model. *J Alzheimers Dis* (2016) 50 (4):1227–41. doi: 10.3233/JAD-150652
- White MR, Kandel R, Tripathi S, Condon D, Qi L, Taubenberger J, et al. Alzheimer's Associated β -Amyloid Protein Inhibits Influenza A Virus and Modulates Viral Interactions With Phagocytes. *PLoS One* (2014) 9(7):e101364. doi: 10.1371/journal.pone.0101364
- Martin C, Aguila B, Araya P, Vio K, Valdivia S, Zambrano A, et al. Inflammatory and Neurodegeneration Markers During Asymptomatic HSV-1 Reactivation. *J Alzheimers Dis* (2014) 39(4):849–59. doi: 10.3233/JAD-131706
- De Chiara G, Piacentini R, Fabiani M, Mastrodonato A, Marcocci ME, Limongi D, et al. Recurrent Herpes Simplex Virus-1 Infection Induces Hallmarks of Neurodegeneration and Cognitive Deficits in Mice. *PLoS Pathog* (2019) 15(3):e1007617. doi: 10.1371/journal.ppat.1007617
- Lövheim H, Gilthorpe J, Adolfsson R, Nilsson LG, Elgh F. Reactivated Herpes Simplex Infection Increases the Risk of Alzheimer's Disease. *Alzheimers Dement* (2015) 11(6):593–9. doi: 10.1016/j.jalz.2014.04.522
- Letenneur L, Pèrès K, Fleury H, Garrigue I, Barberger-Gateau P, Helmer C, et al. Seropositivity to Herpes Simplex Virus Antibodies and Risk of Alzheimer's Disease: A Population-Based Cohort Study. *PLoS One* (2008) 3 (11):e3637. doi: 10.1371/journal.pone.0003637
- Halford WP, Gebhardt BM, Carr DJ. Persistent Cytokine Expression in Trigeminal Ganglion Latently Infected With Herpes Simplex Virus Type 1. *J Immunol* (1996) 157(8):3542–9.
- Cantin EM, Hinton DR, Chen J, Openshaw H. Gamma Interferon Expression During Acute and Latent Nervous System Infection by Herpes Simplex Virus Type 1. *J Virol* (1995) 69(8):4898–905. doi: 10.1128/JVI.69.8.4898-4905.1995
- Wilson NS, Duestell P, Yang B, Li Y, Marsters S, Koernig S, et al. Inflammasome-Dependent and -Independent IL-18 Production Mediates Immunity to the ISCOMATRIX Adjuvant. *J Immunol* (2014) 192(7):3259–68. doi: 10.4049/jimmunol.1302011
- Norkiene M, Stonyte J, Ziogiene D, Mazeika E, Sasnauskas K, Gedvilaite A. Production of Recombinant VP1-Derived Virus-Like Particles From Novel Human Polyomaviruses in Yeast. *BMC Biotechnol* (2015) 15:68. doi: 10.1186/s12896-015-0187-z
- Samuel D, Sasnauskas K, Jin L, Gedvilaite A, Slibinskas R, Beard S, et al. Development of a Measles Specific IgM ELISA for Use With Serum and Oral Fluid Samples Using Recombinant Measles Nucleoprotein Produced in *Saccharomyces Cerevisiae*. *J Clin Virol* (2003) 28(2):121–9. doi: 10.1016/s1386-6532(02)00273-1
- Zvirbliene A, Kucinskaitė I, Sezaite I, Samuel D, Sasnauskas K. Mapping of B Cell Epitopes in Measles Virus Nucleocapsid Protein. *Arch Virol* (2007) 152 (1):25–39. doi: 10.1007/s00705-006-0837-5
- Chanput W, Mes JJ, Wichers HJ. THP-1 Cell Line: An *In Vitro* Cell Model for Immune Modulation Approach. *Int Immunopharmacol* (2014) 23(1):37–45. doi: 10.1016/j.intimp.2014.08.002
- Samuel D, Sasnauskas K, Jin L, Beard S, Zvirbliene A, Gedvilaite A, et al. High Level Expression of Recombinant Mumps Nucleoprotein in

- Saccharomyces Cerevisiae and its Evaluation in Mumps IgM Serology. *J Med Virol* (2002) 66(1):123–30. doi: 10.1002/jmv.2120
41. Slibinskas R, Samuel D, Gedvilaite A, Staniulis J, Sasnauskas K. Synthesis of the Measles Virus Nucleoprotein in Yeast *Pichia Pastoris* and *Saccharomyces Cerevisiae*. *J Biotechnol* (2004) 107(2):115–24. doi: 10.1016/j.jbiotec.2003.10.018
 42. Klein AM, Mazutis L, Akartuna I, Tallapragada N, Veres A, Li V, et al. Droplet Barcoding for Single-Cell Transcriptomics Applied to Embryonic Stem Cells. *Cell* (2015) 161(5):1187–201. doi: 10.1016/j.cell.2015.04.044
 43. Zilionis R, Nainys J, Veres A, Savova V, Zemmour D, Klein AM, et al. Single-Cell Barcoding and Sequencing Using Droplet Microfluidics. *Nat Protoc* (2017) 12(1):44–73. doi: 10.1038/nprot.2016.154
 44. Hashimshony T, Wagner F, Sher N, Yanai I. CEL-Seq: Single-Cell RNA-Seq by Multiplexed Linear Amplification. *Cell Rep* (2012) 2(3):666–73. doi: 10.1016/j.celrep.2012.08.003
 45. Ramsköld D, Luo S, Wang YC, Li R, Deng Q, Faridani OR, et al. Full-Length mRNA-Seq From Single-Cell Levels of RNA and Individual Circulating Tumor Cells. *Nat Biotechnol* (2012) 30(8):777–82. doi: 10.1038/nbt.2282
 46. Becht E, McInnes L, Healy J, Dutertre CA, Kwok IWH, Ng LG, et al. Dimensionality Reduction for Visualizing Single-Cell Data Using UMAP. *Nat Biotechnol* (2019) 37:38–44. doi: 10.1038/nbt.4314
 47. Franklin BS, Latz E, Schmidt FI. The Intra- and Extracellular Functions of ASC Specks. *Immunol Rev* (2018) 281(1):74–87. doi: 10.1111/imr.12611
 48. Luecken MD, Theis FJ. Current Best Practices in Single-Cell RNA-Seq Analysis: A Tutorial. *Mol Syst Biol* (2019) 15(6):e8746. doi: 10.15252/msb.20188746
 49. Weinreb C, Wolock S, Klein AM. SPRING: A Kinetic Interface for Visualizing High Dimensional Single-Cell Expression Data. *Bioinformatics* (2018) 34(7):1246–8. doi: 10.1093/bioinformatics/btx792
 50. Rashidi M, Bandala-Sanchez E, Lawlor KE, Zhang Y, Neale AM, Vijayaraj SL, et al. CD52 Inhibits Toll-Like Receptor Activation of NF- κ B and Triggers Apoptosis to Suppress Inflammation. *Cell Death Differ* (2018) 25(2):392–405. doi: 10.1038/cdd.2017.173
 51. Galati D, Srinivasan S, Raza H, Prabu SK, Hardy M, Chandran K, et al. Role of Nuclear-Encoded Subunit Vb in the Assembly and Stability of Cytochrome C Oxidase Complex: Implications in Mitochondrial Dysfunction and ROS Production. *Biochem J* (2009) 420(3):439–49. doi: 10.1042/BJ20090214
 52. Lu Z, Lam KS, Wang N, Xu X, Cortes M, Andersen B. LMO4 can Interact With Smad Proteins and Modulate Transforming Growth Factor-Beta Signaling in Epithelial Cells. *Oncogene* (2006) 25(20):2920–30. doi: 10.1038/sj.onc.1209318
 53. Maeda M, Hasegawa H, Hyodo T, Ito S, Asano E, Yuang H, et al. ARHGAP18, a GTPase-Activating Protein for RhoA, Controls Cell Shape, Spreading, and Motility. *Mol Biol Cell* (2011) 22(20):3840–52. doi: 10.1091/mb.E11-04-0364
 54. Liu L, Zhang J, Li S, Yin L, Tai J. Silencing of TMEM158 Inhibits Tumorigenesis and Multidrug Resistance in Colorectal Cancer. *Nutr Cancer* (2020) 72(4):662–71. doi: 10.1080/01635581.2019.1650192
 55. Cheng Z, Guo J, Chen L, Luo N, Yang W, Qu X. Overexpression of TMEM158 Contributes to Ovarian Carcinogenesis. *J Exp Clin Cancer Res* (2015) 34:75. doi: 10.1186/s13046-015-0193-y
 56. Satoh J, Kino Y, Asahina N, Takitani M, Miyoshi J, Ishida T, et al. TMEM119 Marks a Subset of Microglia in the Human Brain. *Neuropathology* (2016) 36(1):39–49. doi: 10.1111/neup.12235
 57. Butovsky O, Jedrychowski MP, Moore CS, Cialic R, Lanser AJ, Gabriely G, et al. Identification of a Unique TGF- β -Dependent Molecular and Functional Signature in Microglia. *Nat Neurosci* (2014) 17(1):131–43. doi: 10.1038/nn.3599
 58. Mastroberardino PG, Iannicola C, Nardacci R, Bernassola F, De Laurenzi V, Melino G, et al. 'Tissue' Transglutaminase Ablation Reduces Neuronal Death and Prolongs Survival in a Mouse Model of Huntington's Disease. *Cell Death Differ* (2002) 9(9):873–80. doi: 10.1038/sj.cdd.4401093
 59. Wang J, Rousseau J, Kim E, Ehresmann S, Cheng YT, Duraine L, et al. Loss of Oxidation Resistance 1, OXR1, Is Associated With an Autosomal-Recessive Neurological Disease With Cerebellar Atrophy and Lysosomal Dysfunction. *Am J Hum Genet* (2019) 105(6):1237–53. doi: 10.1016/j.ajhg.2019.11.002
 60. Volkert MR, Elliott NA, Housman DE. Functional Genomics Reveals a Family of Eukaryotic Oxidation Protection Genes. *Proc Natl Acad Sci USA* (2000) 97(26):14530–5. doi: 10.1073/pnas.260495897
 61. Kornblihtt AR, Gutman A. Molecular Biology of the Extracellular Matrix Proteins. *Biol Rev Camb Philos Soc* (1988) 63(4):465–507. doi: 10.1111/j.1469-185x.1988.tb00668.x
 62. Hynes RO. Fibronectins. *Sci Am* (1986) 254(6):42–51. doi: 10.1038/scientificamerican0686-42
 63. Osellame LD, Blacker TS, Duchon MR. Cellular and Molecular Mechanisms of Mitochondrial Function. *Best Pract Res Clin Endocrinol Metab* (2012) 26(6):711–23. doi: 10.1016/j.beem.2012.05.003
 64. Kominami E, Ishido K, Muno D, Sato N. The Primary Structure and Tissue Distribution of Cathepsin C. *Biol Chem Hoppe Seyler* (1992) 373(7):367–73. doi: 10.1515/bchm3.1992.373.2.367
 65. Rabolli V, Lison D, Huaux F. The Complex Cascade of Cellular Events Governing Inflammasome Activation and IL-1 β Processing in Response to Inhaled Particles. *Part Fibre Toxicol* (2016) 13(1):40. doi: 10.1186/s12989-016-0150-8
 66. Alam S, Liu Q, Liu S, Liu Y, Zhang Y, Yang X, et al. Up-Regulated Cathepsin C Induces Macrophage M1 Polarization Through FAK-Triggered P38 MAPK/NF- κ B Pathway. *Exp Cell Res* (2019) 382(2):11472. doi: 10.1016/j.yexcr.2019.06.017
 67. Liu Q, Zhang Y, Liu S, Liu Y, Yang X, Liu G, et al. Cathepsin C Promotes Microglia M1 Polarization and Aggravates Neuroinflammation via Activation of Ca. *J Neuroinflamm* (2019) 16(1):10. doi: 10.1186/s12974-019-1398-3
 68. Helfman DM, Kim EJ, Lukanidin E, Grigorian M. The Metastasis Associated Protein S100A4: Role in Tumour Progression and Metastasis. *Br J Cancer* (2005) 92(11):1955–8. doi: 10.1038/sj.bjc.6602613
 69. Hansen MT, Forst B, Cremers N, Quagliata L, Ambartsumian N, Grum-Schwensen B, et al. A Link Between Inflammation and Metastasis: Serum Amyloid A1 and A3 Induce Metastasis, and Are Targets of Metastasis-Inducing S100A4. *Oncogene* (2015) 34(4):424–35. doi: 10.1038/onc.2013.568
 70. Wang KX, Denhardt DT. Osteopontin: Role in Immune Regulation and Stress Responses. *Cytokine Growth Factor Rev* (2008) 19(5-6):333–45. doi: 10.1016/j.cytogfr.2008.08.001
 71. Bouchon A, Hernández-Munain C, Cella M, Colonna M. A DAP12-Mediated Pathway Regulates Expression of CC Chemokine Receptor 7 and Maturation of Human Dendritic Cells. *J Exp Med* (2001) 194(8):1111–22. doi: 10.1084/jem.194.8.1111
 72. Kobayashi M, Konishi H, Sayo A, Takai T, Kiyama H. TREM2/DAP12 Signal Elicits Proinflammatory Response in Microglia and Exacerbates Neuropathic Pain. *J Neurosci* (2016) 36(43):11138–50. doi: 10.1523/JNEUROSCI.1238-16.2016
 73. Turnbull IR, Gilfillan S, Cella M, Aoshi T, Miller M, Piccio L, et al. Cutting Edge: TREM-2 Attenuates Macrophage Activation. *J Immunol* (2006) 177(6):3520–4. doi: 10.4049/jimmunol.177.6.3520
 74. Zhong L, Chen XF, Wang T, Wang Z, Liao C, Huang R, et al. Soluble TREM2 Induces Inflammatory Responses and Enhances Microglial Survival. *J Exp Med* (2017) 214(3):597–607. doi: 10.1084/jem.20160844
 75. Takahashi K, Rochford CD, Neumann H. Clearance of Apoptotic Neurons Without Inflammation by Microglial Triggering Receptor Expressed on Myeloid Cells-2. *J Exp Med* (2005) 201(4):647–57. doi: 10.1084/jem.20041611
 76. N'Diaye EN, Branda CS, Branda SS, Nevarez L, Colonna M, Lowell C, et al. TREM-2 (Triggering Receptor Expressed on Myeloid Cells 2) Is a Phagocytic Receptor for Bacteria. *J Cell Biol* (2009) 184(2):215–23. doi: 10.1083/jcb.200808080
 77. Jiang T, Tan L, Zhu XC, Zhang QQ, Cao L, Tan MS, et al. Upregulation of TREM2 Ameliorates Neuropathology and Rescues Spatial Cognitive Impairment in a Transgenic Mouse Model of Alzheimer's Disease. *Neuropsychopharmacology* (2014) 39(13):2949–62. doi: 10.1038/npp.2014.164
 78. Adamik J, Wang KZ, Unlu S, Su AJ, Tannahill GM, Galson DL, et al. Distinct Mechanisms for Induction and Tolerance Regulate the Immediate Early Genes Encoding Interleukin 1 β and Tumor Necrosis Factor α . *PLoS One* (2013) 8(8):e70622. doi: 10.1371/journal.pone.0070622
 79. Tominaga K, Yoshimoto T, Torigoe K, Kurimoto M, Matsui K, Hada T, et al. IL-12 Synergizes With IL-18 or IL-1 β for IFN- γ Production From

- Human T Cells. *Int Immunol* (2000) 12(2):151–60. doi: 10.1093/intimm/12.2.151
80. Shimizu H, Sakimoto T, Yamagami S. Pro-Inflammatory Role of NLRP3 Inflammasome in Experimental Sterile Corneal Inflammation. *Sci Rep* (2019) 9(1):9596. doi: 10.1038/s41598-019-46116-9
 81. Raman D, Sobolik-Delmaire T, Richmond A. Chemokines in Health and Disease. *Exp Cell Res* (2011) 317(5):575–89. doi: 10.1016/j.yexcr.2011.01.005
 82. Schutyser E, Struyf S, Proost P, Opdenakker G, Laureys G, Verhasselt B, et al. Identification of Biologically Active Chemokine Isoforms From Ascitic Fluid and Elevated Levels of CCL18/pulmonary and Activation-Regulated Chemokine in Ovarian Carcinoma. *J Biol Chem* (2002) 277(27):24584–93. doi: 10.1074/jbc.M112275200
 83. Cook DN. The Role of MIP-1 Alpha in Inflammation and Hematopoiesis. *J Leukoc Biol* (1996) 59(1):61–6. doi: 10.1002/jlb.59.1.61
 84. Ito T, Carson WF, Cavassani KA, Connett JM, Kunkel SL. CCR6 as a Mediator of Immunity in the Lung and Gut. *Exp Cell Res* (2011) 317(5):613–9. doi: 10.1016/j.yexcr.2010.12.018
 85. Pavlova A, Krupa JC, Mort JS, Abrahamson M, Björk I. Cystatin Inhibition of Cathepsin B Requires Dislocation of the Proteinase Occluding Loop. Demonstration By Release of Loop Anchoring Through Mutation of His110. *FEBS Lett* (2000) 487(2):156–60. doi: 10.1016/s0014-5793(00)02337-1
 86. MRSchtik M, Ryan KM. Lysosomal Proteins in Cell Death and Autophagy. *MRS J* (2015) 282(10):1858–70. doi: 10.1111/febs.13253
 87. Chang AC, Jellinek DA, Reddel RR. Mammalian Stanniocalcins and Cancer. *Endocr Relat Cancer* (2003) 10(3):359–73. doi: 10.1677/erc.0.0100359
 88. Leung CCT, Wong CKC. Characterization of Stanniocalcin-1 Expression in Macrophage Differentiation. *Transl Oncol* (2021) 14(1):100881. doi: 10.1016/j.tranon.2020.100881
 89. Van Lint P, Libert C. Matrix Metalloproteinase-8: Cleavage Can Be Decisive. *Cytokine Growth Factor Rev* (2006) 17(4):217–23. doi: 10.1016/j.cytogfr.2006.04.001
 90. Wen G, Zhang C, Chen Q, Luong LA, Mustafa A, Ye S, et al. A Novel Role of Matrix Metalloproteinase-8 in Macrophage Differentiation and Polarization. *J Biol Chem* (2015) 290(31):19158–72. doi: 10.1074/jbc.M114.634022
 91. Kurten RC, Cadena DL, Gill GN. Enhanced Degradation of EGF Receptors by a Sorting Nexin, SNX1. *Science* (1996) 272(5264):1008–10. doi: 10.1126/science.272.5264.1008
 92. Carlton J, Bujny M, Rutherford A, Cullen P. Sorting Nexins—Unifying Trends and New Perspectives. *Traffic* (2005) 6(2):75–82. doi: 10.1111/j.1600-0854.2005.00260.x
 93. Ish-Shalom E, Meirou Y, Sade-Feldman M, Kanterman J, Wang L, Mizrahi O, et al. Impaired SNX9 Expression in Immune Cells During Chronic Inflammation: Prognostic and Diagnostic Implications. *J Immunol* (2016) 196(1):156–67. doi: 10.4049/jimmunol.1402877
 94. Wang JT, Kerr MC, Karunaratne S, Jeanes A, Yap AS, Teasdale RD. The SNX-PX-BAR Family in Macropinosytosis: The Regulation of Macropinosome Formation by SNX-PX-BAR Proteins. *PLoS One* (2010) 5(10):e13763. doi: 10.1371/journal.pone.0013763
 95. Canton J. Macropinosytosis: New Insights Into Its Underappreciated Role in Innate Immune Cell Surveillance. *Front Immunol* (2018) 9:2286. doi: 10.3389/fimmu.2018.02286
 96. Brini M, Carafoli E. The Plasma Membrane Ca²⁺ ATPase and the Plasma Membrane Sodium Calcium Exchanger Cooperate in the Regulation of Cell Calcium. *Cold Spring Harb Perspect Biol* (2011) 3(2):a004168. doi: 10.1101/cshperspect.a004168
 97. Murakami T, Ockinger J, Yu J, Byles V, McColl A, Hofer AM, et al. Critical Role for Calcium Mobilization in Activation of the NLRP3 Inflammasome. *Proc Natl Acad Sci USA* (2012) 109(28):11282–7. doi: 10.1073/pnas.1117765109
 98. Gozzelino R, Soares MP. Coupling Heme and Iron Metabolism via Ferritin H Chain. *Antioxid Redox Signal* (2014) 20(11):1754–69. doi: 10.1089/ars.2013.5666
 99. Soares MP, Hamza I. Macrophages and Iron Metabolism. *Immunity* (2016) 44(3):492–504. doi: 10.1016/j.immuni.2016.02.016
 100. Mesquita G, Silva T, Gomes AC, Oliveira PF, Alves MG, Fernandes R, et al. H-Ferritin Is Essential for Macrophages' Capacity to Store or Detoxify Exogenously Added Iron. *Sci Rep* (2020) 10(1):3061. doi: 10.1038/s41598-020-59898-0
 101. Zhao X, Li J, Winkler CA, An P, Guo JT. IFITM Genes, Variants, and Their Roles in the Control and Pathogenesis of Viral Infections. *Front Microbiol* (2018) 9:3228:3228. doi: 10.3389/fmicb.2018.03228
 102. Spence JS, He R, Hoffmann HH, Das T, Thion E, Rice CM, et al. IFITM3 Directly Engages and Shuttles Incoming Virus Particles to Lysosomes. *Nat Chem Biol* (2019) 15(3):259–68. doi: 10.1038/s41589-018-0213-2
 103. Shi G, Kenney AD, Kudryashova E, Zani A, Zhang L, Lai KK, et al. Opposing Activities of IFITM Proteins in SARS-CoV-2 Infection. *EMBO J* (2021) 40(3):e106501. doi: 10.15252/embj.2020106501
 104. Zhou X, Michal JJ, Zhang L, Ding B, Lunney JK, Liu B, et al. Interferon Induced IFIT Family Genes in Host Antiviral Defense. *Int J Biol Sci* (2013) 9(2):200–8. doi: 10.7150/ijbs.5613
 105. Cheriya V, Leaman DW, Borden EC. Emerging Roles of FAM14 Family Members (G1P3/ISG 6-16 and ISG12/IFIT2) in Innate Immunity and Cancer. *J Interferon Cytokine Res* (2011) 31(1):173–81. doi: 10.1089/jir.2010.0105
 106. Sajid M, Ullah H, Yan K, He M, Feng J, Shereen MA, et al. The Functional and Antiviral Activity of Interferon Alpha-Inducible IFI6 Against Hepatitis B Virus Replication and Gene Expression. *Front Immunol* (2021) 12:634937. doi: 10.3389/fimmu.2021.634937
 107. Perng YC, Lenschow DJ. ISG15 in Antiviral Immunity and Beyond. *Nat Rev Microbiol* (2018) 16(7):423–39. doi: 10.1038/s41579-018-0020-5
 108. Sanyal S. How SARS-CoV-2 (COVID-19) Spreads Within Infected Hosts - What We Know So Far. *Emerg Top Life Sci* (2020) 4(4):371–8. doi: 10.1042/ETLS20200165
 109. Yangüez E, García-Culebras A, Frau A, Llompert C, Knobloch KP, Gutierrez-Erlandsson S, et al. ISG15 Regulates Peritoneal Macrophages Functionality Against Viral Infection. *PLoS Pathog* (2013) 9(10):e1003632. doi: 10.1371/journal.ppat.1003632
 110. Baldanta S, Fernández-Escobar M, Acín-Perez R, Albert M, Camafeita E, Jorge I, et al. ISG15 Governs Mitochondrial Function in Macrophages Following Vaccinia Virus Infection. *PLoS Pathog* (2017) 13(10):e1006651. doi: 10.1371/journal.ppat.1006651
 111. Booth V, Keizer DW, Kamphuis MB, Clark-Lewis I, Sykes BD. The CXCR3 Binding Chemokine IP-10/CXCL10: Structure and Receptor Interactions. *Biochemistry* (2002) 41(33):10418–25. doi: 10.1021/bi026020q
 112. Gasperini S, Marchi M, Calzetti F, Laudanna C, Vicentini L, Olsen H, et al. Gene Expression and Production of the Monokine Induced by IFN- γ (MIG), IFN-Inducible T Cell Alpha Chemoattractant (I-TAC), and IFN- γ -Inducible Protein-10 (IP-10) Chemokines by Human Neutrophils. *J Immunol* (1999) 162(8):4928–37.
 113. Callahan V, Hawks S, Crawford MA, Lehman CW, Morrison HA, Ivester HM, et al. The Pro-Inflammatory Chemokines CXCL9, CXCL10 and CXCL11 Are Upregulated Following SARS-CoV-2 Infection in an AKT-Dependent Manner. *Viruses* (2021) 13(6):1062. doi: 10.3390/v13061062
 114. Vaine CA, Patel MK, Zhu JT, Lee E, Finberg RW, Hayward RC, et al. Tuning Innate Immune Activation by Surface Texturing of Polymer Microparticles: The Role of Shape in Inflammasome Activation. *J Immunol* (2013) 190(7):3525–32. doi: 10.4049/jimmunol.1200492
 115. Halle A, Hornung V, Petzold GC, Stewart CR, Monks BG, Reinheckel T, et al. The NALP3 Inflammasome Is Involved in the Innate Immune Response to Amyloid-Beta. *Nat Immunol* (2008) 9(8):857–65. doi: 10.1038/ni.1636
 116. Pike AF, Varanita T, Herrebout MAC, Plug BC, Kole J, Musters RJP, et al. α -Synuclein Evokes NLRP3 Inflammasome-Mediated IL-1 β Secretion From Primary Human Microglia. *Glia* (2021) 69(6):1413–28. doi: 10.1002/glia.23970
 117. Pan P, Shen M, Yu Z, Ge W, Chen K, Tian M, et al. SARS-CoV-2 N Protein Promotes NLRP3 Inflammasome Activation to Induce Hyperinflammation. *Nat Commun* (2021) 12(1):4664. doi: 10.1038/s41467-021-25015-6
 118. Ma J, Zhu F, Zhao M, Shao F, Yu D, Zhang X, et al. SARS-CoV-2 Nucleocapsid Suppresses Host Pyroptosis by Blocking Gasdermin D Cleavage. *EMBO J* (2021) 40(18):e108249. doi: 10.15252/embj.2021108249
 119. Kelley N, Jeltama D, Duan Y, He Y. The NLRP3 Inflammasome: An Overview of Mechanisms of Activation and Regulation. *Int J Mol Sci* (2019) 20(13):3328. doi: 10.3390/ijms20133328
 120. Neu U, Wang J, Macejak D, Garcea RL, Stehle T. Structures of the Major Capsid Proteins of the Human Karolinska Institutet and Washington University Polyomaviruses. *J Virol* (2011) 85(14):7384–92. doi: 10.1128/JVI.00382-11

121. Neu U, Hengel H, Blaum BS, Schowalter RM, Macejak D, Gilbert M, et al. Structures of Merkel Cell Polyomavirus VP1 Complexes Define a Sialic Acid Binding Site Required for Infection. *PLoS Pathog* (2012) 8(7):e1002738. doi: 10.1371/journal.ppat.1002738
122. Hornung V, Bauernfeind F, Halle A, Samstad EO, Kono H, Rock KL, et al. Silica Crystals and Aluminum Salts Activate the NALP3 Inflammasome Through Phagosomal Destabilization. *Nat Immunol* (2008) 9(8):847–56. doi: 10.1038/ni.1631
123. Rashidi M, Wicks IP, Vince JE. Inflammasomes and Cell Death: Common Pathways in Microparticle Diseases. *Trends Mol Med* (2020) 26(11):1003–20. doi: 10.1016/j.molmed.2020.06.005
124. Selkig J, Li N, Hausmann A, Mangan MSJ, Zietek M, Mateus A, et al. Spatiotemporal Proteomics Uncovers Cathepsin-Dependent Macrophage Cell Death During Salmonella Infection. *Nat Microbiol* (2020) 5(9):1119–+. doi: 10.1038/s41564-020-0736-7
125. Stahl-Meyer J, Stahl-Meyer K, Jäättelä M. Control of Mitosis, Inflammation, and Cell Motility by Limited Leakage of Lysosomes. *Curr Opin Cell Biol* (2021) 71:29–37. doi: 10.1016/j.cob.2021.02.003
126. Orłowski GM, Colbert JD, Sharma S, Bogoy M, Robertson SA, Rock KL. Multiple Cathepsins Promote Pro-IL-1 β Synthesis and NLRP3-Mediated IL-1 β Activation. *J Immunol* (2015) 195(4):1685–97. doi: 10.4049/jimmunol.1500509
127. Swanson MEV, Scotter EL, Smyth LCD, Murray HC, Ryan B, Turner C, et al. Identification of a Dysfunctional Microglial Population in Human Alzheimer's Disease Cortex Using Novel Single-Cell Histology Image Analysis. *Acta Neuropathol Commun* (2020) 8(1):170. doi: 10.1186/s40478-020-01047-9
128. Hammond TR, Dufort C, Dissing-Olesen L, Giera S, Young A, Wysoker A, et al. Single-Cell RNA Sequencing of Microglia Throughout the Mouse Lifespan and in the Injured Brain Reveals Complex Cell-State Changes. *Immunity* (2019) 50(1):253–71.e6. doi: 10.1016/j.immuni.2018.11.004
129. Lawlor N, Nehar-Belaid D, Grassmann JDS, Stoeckius M, Smibert P, Stitzel ML, et al. Single Cell Analysis of Blood Mononuclear Cells Stimulated Through Either LPS or Anti-CD3 and Anti-Cd28. *Front Immunol* (2021) 12:636720. doi: 10.3389/fimmu.2021.636720
130. Dinarello CA. Overview of the IL-1 Family in Innate Inflammation and Acquired Immunity. *Immunol Rev* (2018) 281(1):8–27. doi: 10.1111/imr.12621
131. Carta S, Semino C, Sitia R, Rubartelli A. Dysregulated IL-1 β Secretion in Autoinflammatory Diseases: A Matter of Stress? *Front Immunol* (2017) 8:345. doi: 10.3389/fimmu.2017.00345
132. Schett G, Neurath MF. Resolution of Chronic Inflammatory Disease: Universal and Tissue-Specific Concepts. *Nat Commun* (2018) 9(1):3261. doi: 10.1038/s41467-018-05800-6
133. Fenster V, Sen GC. Interferon-Induced Ifit Proteins: Their Role in Viral Pathogenesis. *J Virol* (2015) 89(5):2462–8. doi: 10.1128/JVI.02744-14
134. Lester SN, Li K. Toll-Like Receptors in Antiviral Innate Immunity. *J Mol Biol* (2014) 426(6):1246–64. doi: 10.1016/j.jmb.2013.11.024
135. Velupillai P, Garcea RL, Benjamin TL. Polyoma Virus-Like Particles Elicit Polarized Cytokine Responses in APCs From Tumor-Susceptible and -Resistant Mice. *J Immunol* (2006) 176(2):1148–53. doi: 10.4049/jimmunol.176.2.1148
136. Scheiblich H, Bousset L, Schwartz S, Griep A, Latz E, Melki R, et al. Microglial NLRP3 Inflammasome Activation Upon TLR2 and TLR5 Ligation by Distinct α -Synuclein Assemblies. *J Immunol* (2021) 207(8):2143–54. doi: 10.4049/jimmunol.2100035
137. Yang R, Wheeler CM, Chen X, Uematsu S, Takeda K, Akira S, et al. Papillomavirus Capsid Mutation to Escape Dendritic Cell-Dependent Innate Immunity in Cervical Cancer. *J Virol* (2005) 79(11):6741–50. doi: 10.1128/JVI.79.11.6741-6750.2005
138. Yang R, Murillo FM, Cui H, Blosser R, Uematsu S, Takeda K, et al. Papillomavirus-Like Particles Stimulate Murine Bone Marrow-Derived Dendritic Cells to Produce Alpha Interferon and Th1 Immune Responses via Myd88. *J Virol* (2004) 78(20):11152–60. doi: 10.1128/JVI.78.20.11152-11160.2004
139. Cai M, Li M, Wang K, Wang S, Lu Q, Yan J, et al. The Herpes Simplex Virus 1-Encoded Envelope Glycoprotein B Activates NF- κ B Through the Toll-Like Receptor 2 and MyD88/TRAF6-Dependent Signaling Pathway. *PLoS One* (2013) 8(1):e54586. doi: 10.1371/journal.pone.0054586
140. Leoni V, Gianni T, Salvioli S, Campadelli-Fiume G. Herpes Simplex Virus Glycoproteins Gh/gL and gB Bind Toll-Like Receptor 2, and Soluble Gh/gL is Sufficient to Activate NF- κ B. *J Virol* (2012) 86(12):6555–62. doi: 10.1128/JVI.00295-12
141. Boehme KW, Guerrero M, Compton T. Human Cytomegalovirus Envelope Glycoproteins B and H are Necessary for TLR2 Activation in Permissive Cells. *J Immunol* (2006) 177(10):7094–102. doi: 10.4049/jimmunol.177.10.7094
142. Kayesh MEH, Kohara M, Tsukiyama-Kohara K. Recent Insights Into the Molecular Mechanism of Toll-Like Receptor Response to Dengue Virus Infection. *Front Microbiol* (2021) 12:744233. doi: 10.3389/fmicb.2021.744233
143. Dolganiuc A, Oak S, Kodys K, Golenbock DT, Finberg RW, Kurt-Jones E, et al. Hepatitis C Core and Nonstructural 3 Proteins Trigger Toll-Like Receptor 2-Mediated Pathways and Inflammatory Activation. *Gastroenterology* (2004) 127(5):1513–24. doi: 10.1053/j.gastro.2004.08.067
144. Negash AA, Olson RM, Griffin S, Gale M. Modulation of Calcium Signaling Pathway by Hepatitis C Virus Core Protein Stimulates NLRP3 Inflammasome Activation. *PLoS Pathog* (2019) 15(2):e1007593. doi: 10.1371/journal.ppat.1007593
145. Pollard AJ, Bijker EM. A Guide to Vaccinology: From Basic Principles to New Developments. *Nat Rev Immunol* (2021) 21(2):83–100. doi: 10.1038/s41577-020-00479-7

Conflict of Interest: RŽ and AŠ are employed at Droplet Genomics. RŽ is a shareholder at Droplet Genomics. These commercial relationships are unrelated to the current study.

The remaining authors declare that the research was conducted in the absence of any commercial or financial relationships that could be construed as a potential conflict of interest.

Publisher's Note: All claims expressed in this article are solely those of the authors and do not necessarily represent those of their affiliated organizations, or those of the publisher, the editors and the reviewers. Any product that may be evaluated in this article, or claim that may be made by its manufacturer, is not guaranteed or endorsed by the publisher.

Copyright © 2022 Lučičunaitė, Dalgėdienė, Žilionis, Mašalaitė, Norkienė, Šinkūnas, Gedvilaitė, Kučinskaitė-Kodžė and Žvirblienė. This is an open-access article distributed under the terms of the Creative Commons Attribution License (CC BY). The use, distribution or reproduction in other forums is permitted, provided the original author(s) and the copyright owner(s) are credited and that the original publication in this journal is cited, in accordance with accepted academic practice. No use, distribution or reproduction is permitted which does not comply with these terms.